
Collapsing Taylor Mode Automatic Differentiation

Felix Dangel*
Vector Institute
Toronto, Canada
fdangel@vectorinstitute.ai

Tim Siebert*
Humboldt-Universität zu Berlin and
Zuse Institute Berlin
Berlin, Germany
tim.siebert@hu-berlin.de

Marius Zeinhofer
ETH Zurich
Zurich, Switzerland,
marius.zeinhofer@sam.math.ethz.ch

Andrea Walther
Humboldt-Universität zu Berlin and
Zuse Institute Berlin
Berlin, Germany
andrea.walther@math.hu-berlin.de

Abstract

Computing partial differential equation (PDE) operators via nested backpropagation is expensive, yet popular, and severely restricts their utility for scientific machine learning. Recent advances, like the forward Laplacian and randomizing Taylor mode automatic differentiation (AD), propose forward schemes to address this. We introduce an optimization technique for Taylor mode that “collapses” derivatives by rewriting the computational graph, and demonstrate how to apply it to general linear PDE operators, and randomized Taylor mode. The modifications simply require propagating a sum up the computational graph, which could—or should—be done by a machine learning compiler, without exposing complexity to users. We implement our collapsing procedure and evaluate it on popular PDE operators, confirming it accelerates Taylor mode and outperforms nested backpropagation.

1 Introduction

Using neural networks to learn functions constrained by physical laws is a popular trend in scientific machine learning [4, 16, 17, 19, 24, 25, 29]. Typically, the Physics is encoded through partial differential equations (PDEs) that the neural net must satisfy. The associated loss functions require evaluating differential operators w.r.t. the net’s input, rather than weights. Evaluating these differential operators remains a computational challenge, especially if they contain high-order derivatives.

Computing PDE operators. Two important fields that build on PDE operators are variational Monte-Carlo (VMC) simulations and Physics-informed neural networks (PINNs). VMC employs neural networks as ansatz for the Schrödinger equation [4, 16, 24] and demands computing the net’s Laplacian (the Hessian trace) for the Hamiltonian’s kinetic term. PINNs represent PDE solutions as a neural net and train it by minimizing the residuals of the governing equations [19, 25]. For instance, Kolmogorov-type equations like the Fokker-Planck and Black-Scholes equation require weighted second-order derivatives on high-dimensional spatial domains [17, 28]. Other PINNs for elasticity problems use the biharmonic operator [7, 17, 27, 31], which contains fourth-order derivatives.

Is backpropagation all we need? Although nesting first-order automatic differentiation (AD) to compute high-order derivatives scales exponentially w.r.t. the degree in time and memory [27, §3.2],

*Equal contribution

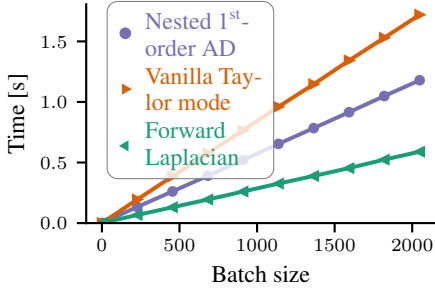
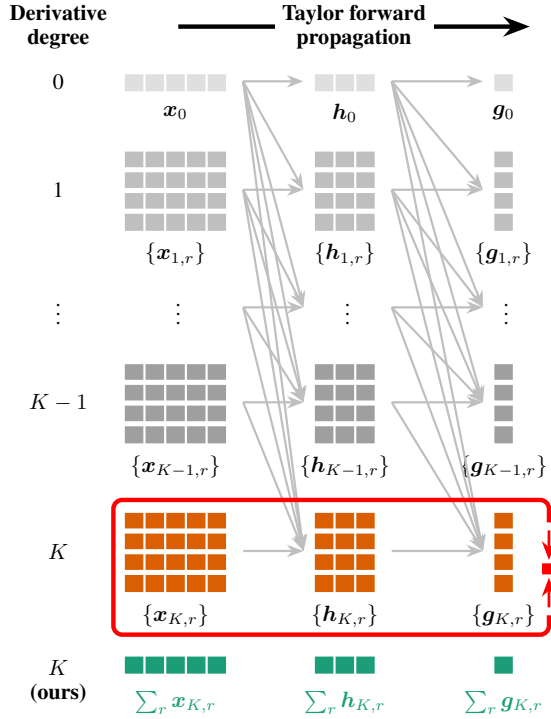


Figure 1: **▲ Vanilla Taylor mode is not enough to beat nested 1st-order AD.** Illustrated for computing the Laplacian of a \tanh -activated $50 \rightarrow 768 \rightarrow 768 \rightarrow 512 \rightarrow 512 \rightarrow 1$ MLP with JAX (+ `jit`) on GPU (details in §G). We show how to automatically obtain the specialized forward Laplacian through simple graph transformations that “collapse” vanilla Taylor mode.

Figure 2: **► Collapsed Taylor mode directly propagates the sum of highest degree coefficients.** Visualized for pushing 4 K -jets through a $\mathbb{R}^5 \rightarrow \mathbb{R}^3 \rightarrow \mathbb{R}$ function ($K = 2$ yields the forward Laplacian).



this approach is common practice: it is easy to implement in ML libraries, and their backpropagation is highly optimized. A promising alternative is *Taylor mode AD* [or simply *Taylor mode*, 13, §13], introduced to the ML community in 2019, which scales polynomially w.r.t. the degree in time and memory [14]. However, we observe empirically that vanilla Taylor mode may not be enough to beat nesting (fig. 1): evaluating the Laplacian of a 5-layer MLP, using JAX’s *Taylor mode* is 50% slower than *nested backpropagation* that computes, then traces, the Hessian via Hessian-vector products [23]. This calls into question the relevance of Taylor mode for computing common PDE operators.

The advent of forward schemes. Recent works have successfully demonstrated the potential of modified forward propagation schemes, though. For the Laplacian, Li et al. [20, 21] developed a special forward propagation framework called the *forward Laplacian*, whose JAX implementation [12] is *roughly twice as fast as nested first-order AD* (fig. 1). While the forward Laplacian does not rely on Taylor mode, recent work pointed out a connection [6]; it remains unclear, though, if efficient forward schemes exist for other differential operators, and how they relate to Taylor mode. Concurrently, Shi et al. [27] derived stochastic approximations of differential operators in high dimensions by evaluating Taylor mode along suitably sampled random directions.

Irrespective of stochastic or exact computation, at their core, these popular PDE operators are *linear*: we must evaluate derivatives along multiple directions, then sum them. Based on this linearity, we identify an optimization technique to rewrite the computational graph of standard Taylor mode that is applicable to general linear PDE operators and randomized Taylor mode:

1. **We propose optimizing standard Taylor mode by collapsing the highest Taylor coefficients,** directly **propagating their sum**, rather than **propagating then summing** (fig. 2). Our approach contains the forward Laplacian as special case, is applicable to randomized Taylor mode, and also general linear PDE operators, which we show using the techniques from Griewank et al. [14].
2. **We show how to collapse standard Taylor mode by simple graph rewrites based on linearity.** This leads to a clean separation of concepts: Users can build their computational graph using standard Taylor mode, then rewrite it to collapse it. Due to the simple nature of our proposed rewrites, they could easily be absorbed into the just-in-time (JIT) compilation of ML frameworks without introducing a new interface or exposing complexity to users.

3. **We empirically demonstrate that collapsing Taylor mode accelerates standard Taylor mode.** We implement a Taylor mode library² for PyTorch [22] that realizes the graph simplifications with `torch.fx` [26]. On popular PDE operators, we empirically find that, compared to standard Taylor mode, collapsed Taylor mode achieves superior performance that is well-aligned with the theoretical expectation, while consistently outperforming nested first-order AD.

Our work takes an important step towards the broader adoption of Taylor mode as viable alternative to nested first-order AD for computing PDE operators, while being as easy to use.

2 Background: Introduction to Taylor Mode AD

Taylor mode AD (or, simply, Taylor mode) computes higher-order derivatives—as needed, e.g., for PDE operators—through propagation of Taylor coefficients according to the chain rule.

Scalar case. To illustrate Taylor mode, consider the scalar function $f : \mathbb{R} \rightarrow \mathbb{R}$ and extend the input variable x to a path $x(t)$ with $x(0) = x_0$, whose form is a univariate Taylor polynomial of degree K , $x(t) = \sum_{k=0}^K \frac{t^k}{k!} x_k$ with x_k the k -th Taylor coefficient. If f is smooth enough, we can evaluate Taylor coefficients of the transformed path $f(x(t)) = \sum_{k=0}^K \frac{t^k}{k!} f_k$ with $f_k := \frac{d^k}{dt^k} f(x(t))|_{t=0}$. The chain rule provides the coefficients’ propagation rules. E.g., for degree $K = 3$ we get

$$\begin{aligned} f_0 &= f(x_0), & f_2 &= \partial^2 f(x_0) x_1^2 + \partial f(x_0) x_2, \\ f_1 &= \partial f(x_0) x_1, & f_3 &= \partial^3 f(x_0) x_1^3 + 3\partial^2 f(x_0) x_1 x_2 + \partial f(x_0) x_3. \end{aligned} \quad (1)$$

Faà Di Bruno [9] provided the general formula for f_k , and Fraenkel [11] extended it to the multivariate case [see also 1, 15]. It serves as foundation for Taylor mode to compute higher-order derivatives [e.g., 13, §13]: setting $x_1 = 1, x_2 = x_3 = 0$ yields $f_1 = \partial f(x_0), f_2 = \partial^2 f(x_0), f_3 = \partial^3 f(x_0)$. We call the univariate Taylor polynomial of a function $x(t)$ of degree K , represented by the coefficients (x_0, \dots, x_K) , the K -jet of x , following the terminology of JAX’s Taylor mode [2].

Notation for multivariate case. We consider the general case of computing higher-order derivatives, e.g., PDE operators, of a vector-to-vector function $\mathbf{f} : \mathbb{R}^D \rightarrow \mathbb{R}^C$. This requires additional notation to generalize eq. (1). Given K vectors $\mathbf{v}_1, \dots, \mathbf{v}_K \in \mathbb{R}^D$, we write their tensor product as

$$\otimes_{k=1}^K \mathbf{v}_k = \mathbf{v}_1 \otimes \dots \otimes \mathbf{v}_K \in (\mathbb{R}^D)^{\otimes K} \quad \text{with entries} \quad [\otimes_{k=1}^K \mathbf{v}_k]_{d_1, \dots, d_K} = [\mathbf{v}_1]_{d_1} \dots [\mathbf{v}_K]_{d_K}$$

for $d_1, \dots, d_K \in \{1, \dots, D\}$, and compactly write $\mathbf{v}^{\otimes K} = \otimes_{k=1}^K \mathbf{v}$. We define the inner product of two tensors $\mathbf{A}, \mathbf{B} \in (\mathbb{R}^D)^{\otimes K}$ as the Euclidean inner product of their flattened versions

$$\langle \mathbf{A}, \mathbf{B} \rangle := \sum_{d_1} \sum_{d_2} \dots \sum_{d_K} [\mathbf{A}]_{d_1, d_2, \dots, d_K} [\mathbf{B}]_{d_1, d_2, \dots, d_K} \in \mathbb{R}. \quad (2)$$

We allow broadcasting in eq. (2): if one tensor has more dimensions but matching trailing dimensions, we take the inner product for each component of the leading dimensions. This allows to express contractions with derivative tensors of vector-valued functions, e.g., contracting the k -th derivative tensor $\partial^k \mathbf{f}(x_0) \in \mathbb{R}^C \times (\mathbb{R}^D)^{\otimes k}$, such that $\langle \mathbf{A}, \partial^k \mathbf{f}(x_0) \rangle \in \mathbb{R}^C$.

Multivariate case & composition. Evaluating the K -jet of \mathbf{f} at $\mathbf{x}_0 \in \mathbb{R}^D$ starts with the extension of \mathbf{x}_0 to a smooth path $\mathbf{x} : \mathbb{R} \rightarrow \mathbb{R}^D$ with $\mathbf{x}(0) = \mathbf{x}_0$. Formally, the K -jet of \mathbf{f} is defined as

$$J^K \mathbf{f} : \mathbb{R} \rightarrow \mathbb{R}^C, \quad (J^K \mathbf{f})(t) := \sum_{k=0}^K \frac{t^k}{k!} \mathbf{f}_k \quad \text{with} \quad \mathbf{f}_k := \frac{d^k}{dt^k} \mathbf{f}(\mathbf{x}(t))|_{t=0}$$

and requires the K -jet of \mathbf{x} , $(J^K \mathbf{x})(t) := \sum_{k=0}^K \frac{t^k}{k!} \mathbf{x}_k$. As we are interested in the coefficients, we will slightly abuse the K -jet as mapping $(\mathbf{x}_0, \dots, \mathbf{x}_K) \mapsto (\mathbf{f}_0, \dots, \mathbf{f}_K)$ (see fig. 3 for an illustration).

As is common for AD, propagating the coefficients is broken down into composing \mathbf{f} of atomic functions with known derivatives and the chain rule. In the simplest case, let $\mathbf{f} = \mathbf{g} \circ \mathbf{h} : \mathbb{R}^D \rightarrow$

²Available at <https://github.com/f-dangel/torch-jet>.

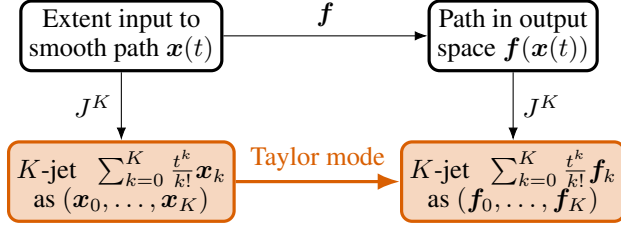


Figure 3: **Taylor mode propagates Taylor coefficients of a path in input space.** This results in the function-transformed path’s Taylor coefficients. The Taylor expansion of degree K is called a K -jet; hence Taylor mode propagates the input K -jet to the output K -jet.

$\mathbb{R}^I \rightarrow \mathbb{R}^C$ for two elemental functions \mathbf{g}, \mathbf{h} . Given the input K -jet for \mathbf{x} , the coefficients $\mathbf{h}_k = \frac{d^k}{dt^k} \mathbf{h}(\mathbf{x}(t))|_{t=0}$ follow from the generalized Faà di Bruno formula (spelled out for some k s in §A)

$$\mathbf{h}_k = \sum_{\sigma \in \text{part}(k)} \nu(\sigma) \left\langle \partial^{|\sigma|} \mathbf{h}, \otimes_{s \in \sigma} \mathbf{x}_s \right\rangle \quad \text{with} \quad \nu(\sigma) = \frac{k!}{(\prod_{s \in \sigma} n_s!) (\prod_{s \in \sigma} s!)} . \quad (3)$$

Here, $\text{part}(k)$ is the integer partitioning of k (a set of sets), ν is a multiplicity function, and n_s counts occurrences of s in a set σ (e.g., $n_1(\{1, 1, 3\}) = 2$ and $n_3 = 1$). Propagating the \mathbf{h}_k s through \mathbf{g} results in the K -jet for \mathbf{f} . In summary, the propagation scheme is (with $\mathbf{x}_k \in \mathbb{R}^D$, $\mathbf{h}_k \in \mathbb{R}^I$, $\mathbf{f}_k \in \mathbb{R}^C$)

$$\begin{aligned} \begin{pmatrix} \mathbf{x}_0 \\ \mathbf{x}_1 \\ \mathbf{x}_2 \\ \vdots \\ \mathbf{x}_K \end{pmatrix} &\stackrel{(3)}{\mapsto} \begin{pmatrix} \mathbf{h}_0 = \mathbf{h}(\mathbf{x}_0) \\ \mathbf{h}_1 = \langle \partial \mathbf{h}(\mathbf{x}_0), \mathbf{x}_1 \rangle \\ \mathbf{h}_2 = \langle \partial^2 \mathbf{h}(\mathbf{x}_0), \mathbf{x}_1^{\otimes 2} \rangle + \langle \partial \mathbf{h}(\mathbf{x}_0), \mathbf{x}_2 \rangle \\ \vdots \\ \mathbf{h}_K = \sum_{\sigma \in \text{part}(K)} \nu(\sigma) \left\langle \partial^{|\sigma|} \mathbf{h}(\mathbf{x}_0), \otimes_{s \in \sigma} \mathbf{x}_s \right\rangle \end{pmatrix} \\ &\stackrel{(3)}{\mapsto} \begin{pmatrix} \mathbf{g}_0 = \mathbf{g}(\mathbf{h}_0) \\ \mathbf{g}_1 = \langle \partial \mathbf{g}(\mathbf{h}_0), \mathbf{h}_1 \rangle \\ \mathbf{g}_2 = \langle \partial^2 \mathbf{g}(\mathbf{h}_0), \mathbf{h}_1^{\otimes 2} \rangle + \langle \partial \mathbf{g}(\mathbf{h}_0), \mathbf{h}_2 \rangle \\ \vdots \\ \mathbf{g}_K = \sum_{\sigma \in \text{part}(K)} \nu(\sigma) \left\langle \partial^{|\sigma|} \mathbf{g}(\mathbf{h}_0), \otimes_{s \in \sigma} \mathbf{h}_s \right\rangle \end{pmatrix} \stackrel{(1)}{=} \begin{pmatrix} \mathbf{f}_0 = \mathbf{f}(\mathbf{x}_0) \\ \mathbf{f}_1 = \langle \partial \mathbf{f}(\mathbf{x}_0), \mathbf{x}_1 \rangle \\ \mathbf{f}_2 = \langle \partial^2 \mathbf{f}(\mathbf{x}_0), \mathbf{x}_1^{\otimes 2} \rangle + \langle \partial \mathbf{f}(\mathbf{x}_0), \mathbf{x}_2 \rangle \\ \vdots \\ \mathbf{f}_K = \sum_{\sigma \in \text{part}(K)} \nu(\sigma) \left\langle \partial^{|\sigma|} \mathbf{f}(\mathbf{x}_0), \otimes_{s \in \sigma} \mathbf{x}_s \right\rangle \end{pmatrix} \end{aligned} \quad (4)$$

which describes the forward propagation of a *single* K -jet. However, computing popular PDE operators requires propagating *multiple* K -jets in parallel, then summing their results. We propose to pull this accumulation inside Taylor mode’s propagation scheme, thereby collapsing it.

3 Collapsing Taylor Mode AD

We now describe how to collapse the Taylor mode AD computation of popular linear PDE operators and their stochastic approximations proposed in [27], and provide a general recipe for computing and collapsing general linear differential operators by interpolation, using earlier work from Griewank et al. [14]. At its core, our procedure uses the linearity of the highest Taylor coefficient’s propagation rule. It allows to collapse coefficients along multiple directions and directly **propagate their sum**, rather than **propagating then summing**, yielding substantial reductions in computational cost.

3.1 Exploiting Linearity to Collapse Taylor Mode AD

To derive our proposed method, we start with a sum of K th-order directional derivatives of the function \mathbf{f} along R directions $\{\mathbf{v}_r\}_{r=1}^R$, which is a common building block for all our PDE operators:

$$\sum_{r=1}^R \langle \partial^K \mathbf{f}(\mathbf{x}_0), \mathbf{v}_r^{\otimes K} \rangle \in \mathbb{R}^C \quad (5)$$

(e.g., the exact Laplacian uses $K = 2$, $R = \dim(\mathbf{x}_0) = D$, and the unit vectors $\mathbf{v}_r = \mathbf{e}_r \in \mathbb{R}^D$ as directions; see §3.2 below). Instead of nesting K calls to 1st-order AD, we can use K -jets to calculate

each summand of eq. (5) with Taylor mode. In total, we need R K -jets, and have to set the r -th jet's coefficients to $\mathbf{x}_{0,r} = \mathbf{x}_0$, $\mathbf{x}_{1,r} = \mathbf{v}_r$ and $\mathbf{x}_{2,r} = \dots = \mathbf{x}_{K,r} = \mathbf{0}$ (eq. (D13) applies this to eq. (4)).

Standard Taylor mode propagates $1 + KR$ vectors through every node of the computational graph (the 0th component is shared across all jets, see fig. 2). This gives the output jets $\{\{\mathbf{f}_{k,r}\}_{k=1}^K\}_{r=1}^R$, from which we only select the highest-degree coefficients $\{\mathbf{f}_{K,r}\}_{r=1}^R$, then sum them to obtain eq. (5).

The approach we propose here exploits that the K -th derivative of $\mathbf{g} \circ \mathbf{h}$ is $\partial \mathbf{g}$ times the K -th derivative of \mathbf{h} plus other lower-order terms in \mathbf{h} . Therefore, $\mathbf{g} \circ \mathbf{h}$ is linear in the K -th derivative of \mathbf{h} . Mathematically speaking, there is a special element in the set of integer partitions $\text{part}(K)$, namely the trivial partition $\tilde{\sigma} = \{K\}$, which contributes the term $\nu(\tilde{\sigma}) \langle \partial \mathbf{g}(\mathbf{h}_0), \mathbf{h}_{K,r} \rangle$ to eq. (3). This is the only term that uses the input jet's highest coefficient $\mathbf{h}_{K,r}$, and its dependency is *linear*. Separating it in the highest coefficient's forward propagation, we get (using $\nu(\tilde{\sigma}) = 1$)

$$\sum_{r=1}^R \mathbf{f}_{K,r} = \sum_{r=1}^R \mathbf{g}_{K,r} = \sum_{r=1}^R \sum_{\sigma \in \text{part}(K) \setminus \{\tilde{\sigma}\}} \nu(\sigma) \left\langle \partial^{|\sigma|} \mathbf{g}(\mathbf{h}_0), \otimes_{s \in \sigma} \mathbf{h}_{s,r} \right\rangle + \sum_{r=1}^R \langle \partial \mathbf{g}(\mathbf{h}_0), \mathbf{h}_{K,r} \rangle$$

and since the propagation rule is linear w.r.t. $\mathbf{h}_{K,r}$, we can pull the summation inside:

$$\sum_{r=1}^R \mathbf{g}_{K,r} = \sum_{r=1}^R \sum_{\sigma \in \text{part}(K) \setminus \{\tilde{\sigma}\}} \nu(\sigma) \left\langle \partial^{|\sigma|} \mathbf{g}(\mathbf{h}_0), \otimes_{s \in \sigma} \mathbf{h}_{s,r} \right\rangle + \left\langle \partial \mathbf{g}(\mathbf{h}_0), \sum_{r=1}^R \mathbf{h}_{K,r} \right\rangle. \quad (6)$$

This is the key insight of our work: *The summed highest-degree output coefficients depend on the summed highest-degree input coefficients* (as well as all lower-degree coefficients). The reason is *linearity* in Faà di Bruno's formula. Hence, to compute the sum $\sum_r \mathbf{g}_{K,r}$ we can directly propagate the sum $\sum_r \mathbf{h}_{K,r}$, collapsing coefficients over all directions. We call this *collapsed Taylor mode AD*.

Collapsed Taylor mode propagates only $1 + (K - 1)R + 1$ vectors through every node in the computational graph (see fig. 2 and eq. (D14) which applies this to eq. (3)). These savings of $R - 1$ coefficients are significant improvements over standard Taylor mode, as we show below. In the following, we discuss how to collapse the Taylor mode computation of various PDE operators.

3.2 Linear Second-order Operators

Laplacian. The Laplace operator plays a central role in Physics and engineering, including electrostatics, fluid dynamics, heat conduction, and quantum mechanics [10, 24]. It contains the Hessian trace of each element of a function, i.e., for $\mathbf{f} : \mathbb{R}^D \rightarrow \mathbb{R}^C$, it is

$$\underbrace{\Delta \mathbf{f}(\mathbf{x}_0)}_{\in \mathbb{R}^C} := \langle \partial^2 \mathbf{f}(\mathbf{x}_0), \mathbf{I}_D \rangle \begin{cases} = \sum_{d=1}^D \langle \partial^2 \mathbf{f}(\mathbf{x}_0), \mathbf{e}_d^{\otimes 2} \rangle & \text{(exact)} \\ \stackrel{[27]}{\approx} \frac{1}{S} \sum_{s=1}^S \langle \partial^2 \mathbf{f}(\mathbf{x}_0), \mathbf{v}_s^{\otimes 2} \rangle & \text{(stochastic)} \end{cases} \quad (7a)$$

with the d -th standard basis vector \mathbf{e}_d used for exact computation, and S random vectors \mathbf{v}_s drawn i.i.d. from a distribution with unit variance (e.g. Rademacher or standard Gaussian) for stochastic estimation. By pattern-matching eq. (7a) with eq. (5) we conclude that $K = 2$, and the following choices for computing the Laplacian with standard Taylor mode:

$$\left. \begin{aligned} \{(\mathbf{x}_{0,d} = \mathbf{x}_0, \quad \mathbf{x}_{1,d} = \mathbf{e}_d, \quad \mathbf{x}_{2,d} = \mathbf{0})\}_{d=1}^D & \quad 1 + D + D \text{ vectors} & \text{(exact)} \\ \{(\mathbf{x}_{0,s} = \mathbf{x}_0, \quad \mathbf{x}_{1,s} = \mathbf{v}_s, \quad \mathbf{x}_{2,s} = \mathbf{0})\}_{s=1}^S & \quad 1 + S + S \text{ vectors} & \text{(stochastic)} \end{aligned} \right\} \quad (7b)$$

Collapsing standard Taylor mode yields $1 + D + 1$ (exact) and $1 + S + 1$ (stochastic) vectors. In fact, the collapsed Taylor mode for the exact Laplacian is the forward Laplacian from Li et al. [21] (see eq. (D16) for detailed presentation of the forward propagation). Note how we can seamlessly also collapse the stochastic approximation over the sampled directions, which is currently not done.

Weighted Laplacian. A natural generalization of the Laplacian involves contracting with a positive semi-definite matrix $\mathbf{D} = \boldsymbol{\sigma} \boldsymbol{\sigma}^\top \in \mathbb{R}^{D \times D}$ rather than the identity. \mathbf{D} may represent the diffusion tensor in Kolmogorov-type PDEs like the Fokker-Planck equation [17], and $\boldsymbol{\sigma}$ can depend on \mathbf{x}_0

[8]. The weighted Laplacian contains the weighted Hessian's trace $\text{Tr}(\boldsymbol{\sigma}\boldsymbol{\sigma}^\top \partial^2[\mathbf{f}]_c)$ for each output element c of \mathbf{f} . If $\text{rank}(\mathbf{D}) = R$ and therefore $\boldsymbol{\sigma} = (\mathbf{s}_1, \dots, \mathbf{s}_R) \in \mathbb{R}^{D \times R}$, it is

$$\underbrace{\Delta_{\mathbf{D}} \mathbf{f}(\mathbf{x}_0)}_{\in \mathbb{R}^C} := \langle \partial^2 \mathbf{f}(\mathbf{x}_0), \mathbf{D} \rangle \begin{cases} = \sum_{r=1}^R \langle \partial^2 \mathbf{f}(\mathbf{x}_0), \mathbf{s}_r^{\otimes 2} \rangle & \text{(exact)} \\ \stackrel{[17]}{\approx} \frac{1}{S} \sum_{s=1}^S \langle \partial^2 \mathbf{f}(\mathbf{x}_0), (\boldsymbol{\sigma} \mathbf{v}_s)^{\otimes 2} \rangle & \text{(stochastic)} \end{cases} \quad (8a)$$

Computing it requires evaluating the following 2-jets with standard Taylor mode:

$$\begin{aligned} \{(\mathbf{x}_{0,r} = \mathbf{x}_0, \quad \mathbf{x}_{1,r} = \mathbf{s}_r, \quad \mathbf{x}_{2,r} = \mathbf{0})\}_{r=1}^R & \quad \mathbf{1} + R + R \text{ vectors} & \text{(exact)} \\ \{(\mathbf{x}_{0,s} = \mathbf{x}_0, \quad \mathbf{x}_{1,s} = \boldsymbol{\sigma} \mathbf{v}_s, \quad \mathbf{x}_{2,s} = \mathbf{0})\}_{s=1}^S & \quad \mathbf{1} + S + S \text{ vectors} & \text{(stochastic)} \end{aligned} \quad (8b)$$

Our collapsed Taylor mode uses $\mathbf{1} + R + \mathbf{1}$ (exact) and $\mathbf{1} + S + \mathbf{1}$ (stochastic) vectors. This yields the modified forward Laplacian from Li et al. [20]; collapsing the stochastic variant speeds up the Hutchinson trace estimator from Hu et al. [17]. For indefinite \mathbf{D} , we can simply apply this scheme to the positive and negative eigen-spaces (however, such weightings are not used in practise).

3.3 Collapsed Taylor Mode for Arbitrary Mixed Partial Derivatives

So far, we discussed operators that result from contracting the second-order derivative tensor with a coefficient matrix (\mathbf{I} or \mathbf{D}) that can conveniently be written as sum of vector outer products. For orders higher than two, the coefficient tensor can in general *not* easily be decomposed as such. Hence, we extend our framework to also cover differential operators containing mixed-partial derivatives by evaluating a suitable family of jets using the interpolation result of Griewank et al. [14]. As illustrative example, we will use the biharmonic operator with a 4-dimensional coefficient tensor:

$$\underbrace{\Delta^2 \mathbf{f}(\mathbf{x}_0)}_{\in \mathbb{R}^C} \begin{cases} = \sum_{d_1=1}^D \sum_{d_2=1}^D \langle \partial^4 \mathbf{f}(\mathbf{x}_0), \mathbf{e}_{d_1}^{\otimes 2} \otimes \mathbf{e}_{d_2}^{\otimes 2} \rangle & \text{(exact)} \\ \stackrel{[27]}{\approx} \frac{1}{3S} \sum_{s=1}^S \langle \partial^4 \mathbf{f}(\mathbf{x}_0), \mathbf{v}_s^{\otimes 4} \rangle & \text{(stochastic)} \end{cases} \quad (9)$$

We can directly collapse the stochastic version: draw S standard normal vectors $\mathbf{v}_1, \dots, \mathbf{v}_S$ and propagate the coefficients $\{(\mathbf{x}_{0,s} = \mathbf{x}_0, \mathbf{x}_{1,s} = \mathbf{v}_s, \mathbf{x}_{2,s} = \mathbf{x}_{3,s} = \mathbf{x}_{4,s} = \mathbf{0})\}_{s=1}^S$. With standard Taylor mode, this uses $\mathbf{1} + 4S$ vectors; collapsed Taylor mode uses $\mathbf{1} + 3S + \mathbf{1}$ vectors. For the exact biharmonic operator, however, we need to develop an approach to compute mixed partials.

General approach. Assume we want to compute a linear differential operator of degree K . We can do so by contracting the K -th order derivative tensor $\partial^K \mathbf{f}(\mathbf{x}_0)$ with a coefficient tensor $\mathbf{C} \in (\mathbb{R}^D)^{\otimes K}$. We can always express this tensor in a tensor product basis, such that

$$\langle \partial^K \mathbf{f}(\mathbf{x}_0), \mathbf{C} \rangle = \sum_{d_1=1}^{D_1} \dots \sum_{d_I=1}^{D_I} \langle \partial^K \mathbf{f}(\mathbf{x}_0), \mathbf{v}_{d_1}^{\otimes i_1} \otimes \dots \otimes \mathbf{v}_{d_I}^{\otimes i_I} \rangle \in \mathbb{R}^C, \quad (10)$$

where the multi-index entries $\mathbf{i} = (i_1, \dots, i_I)$ sum to K and $D_j \leq D$. For the exact biharmonic operator (eq. (9)), we identify $K = 4, I = 2, \mathbf{i} = (2, 2), D_1 = D_2 = D, \mathbf{v}_{d_1} = \mathbf{e}_{d_1}$, and $\mathbf{v}_{d_2} = \mathbf{e}_{d_2}$. From the Faá di Bruno formula, we know that we can only compute terms of the form $\langle \partial^K \mathbf{f}(\mathbf{x}_0), \mathbf{v}^{\otimes K} \rangle$ with a K -jet. The challenge in eq. (10) is that it includes terms where *not* all directions coincide (e.g., for the biharmonic we have $I = 2$ different directions).

Fortunately, Griewank et al. [14] derived an approach to reconstruct such mixed-direction terms by linearly combining a *family* of K -jets that is determined by all vectors $\mathbf{j} \in \mathbb{N}^I$ whose entries sum to K , see fig. 4 for an illustration for the biharmonic (5 members). The K -jets along these directions are then combined with coefficients $\gamma_{\mathbf{i}, \mathbf{j}} \in \mathbb{R}$, whose definition we provide in §E. In summary, we get

$$\langle \partial^K \mathbf{f}(\mathbf{x}_0), \mathbf{v}_{d_1}^{\otimes i_1} \otimes \dots \otimes \mathbf{v}_{d_I}^{\otimes i_I} \rangle = \sum_{\mathbf{j} \in \mathbb{N}^I, \|\mathbf{j}\|_1 = K} \frac{\gamma_{\mathbf{i}, \mathbf{j}}}{K!} \left\langle \partial^K \mathbf{f}(\mathbf{x}_0), \left(\sum_{i=1}^I \mathbf{v}_{d_i} [\mathbf{j}]_i \right)^{\otimes K} \right\rangle. \quad (11)$$

This construction allows us to rewrite eq. (10) as

$$\sum_{d_1=1}^{D_1} \cdots \sum_{d_I=1}^{D_I} \sum_{j \in \mathbb{N}^I, \|j\|_1=K} \frac{\gamma_{i,j}}{K!} \left\langle \partial^K \mathbf{f}(\mathbf{x}_0), \left(\sum_{i=1}^I \mathbf{v}_{d_i}[j]_i \right)^{\otimes K} \right\rangle,$$

and—since the coefficients $\gamma_{i,j}$ only depend on the problem structure (K , I and i) and *not* on the function \mathbf{f} and the directions \mathbf{v}_{d_i} [14]—we can pull out the inner sum to obtain the final expression

$$\sum_{j \in \mathbb{N}^I, \|j\|_1=K} \frac{\gamma_{i,j}}{K!} \sum_{d_1=1}^{D_1} \cdots \sum_{d_I=1}^{D_I} \left\langle \partial^K \mathbf{f}(\mathbf{x}_0), \left(\sum_{i=1}^I \mathbf{v}_{d_i}[j]_i \right)^{\otimes K} \right\rangle. \quad (12)$$

We can evaluate eq. (12) with standard Taylor mode: For each j , compute $\prod_{i=1}^I D_i$ K -jets with coefficients $\mathbf{x}_0, \mathbf{x}_1 = \sum_i \mathbf{v}_{d_i}[j]_i, \mathbf{x}_2 = \dots = \mathbf{x}_K = \mathbf{0}$. The sums from the tensor basis expansion can be collapsed with our proposed optimization, removing $\prod_{i=1}^I D_i$ vectors from the propagation for each j . After repeating for each member j of the interpolation family, we form the linear combination using the $\gamma_{i,j}$ s, which yields the desired differential operator. We can often exploit symmetries in the $\gamma_{i,j}$ s and basis vectors to further reduce the number of K -jets (see §E.1 for a complete example).

Applied to the biharmonic operator. Let us now illustrate the key steps of applying eq. (12) to the exact biharmonic operator eq. (9) (full procedure in §E.1). Figure 4 illustrates the 5 multi-indices j characterizing the 4-jets we need to interpolate $\langle \partial^4 \mathbf{f}(\mathbf{x}_0), e_{d_1}^{\otimes 2} \otimes e_{d_2}^{\otimes 2} \rangle$, and their coefficients $\gamma_{i,j}$. Their definition, see eq. (E17), shows the equality of $\gamma_{i,j}$ for $j = (4, 0)$ and $j = (0, 4)$, as well as $j = (3, 1)$ and $j = (1, 3)$. Exploiting those symmetries reduces the number of interpolation terms from 5 to 3 (eq. (E19)), corresponding to $D + D^2 + D^2$ 4-jets. Removing doubly-computed terms brings down the number of 4-jets to $D + D(D-1) + 1/2 D(D-1)$ (eq. (E21)). Translated to vectors, standard Taylor mode propagates $1 + 4D + 4D(D-1) + 4/2 D(D-1) = 6D^2 - 2D + 1$ vectors. After collapsing, we get $1 + 3D + 1 + 3D(D-1) + 1 + 3/2 D(D-1) + 1 = 9/2 D^2 - 3/2 D + 4$ vectors. This demonstrates the relevance of collapsing: it achieves a 25% reduction in the quadratic coefficient.

Summary & relation to other approaches for computing mixed partials. The scheme we propose based on Griewank et al. [14]’s interpolation result allows to calculate *general* linear differential operators beyond Laplacians, and is amenable to collapsing. Admittedly, eq. (12) seems daunting at first glance. However, it (i) offers a one-fits-all recipe to construct schemes for general linear PDE operators, and (ii) does not use jets of order $K' > K$ to compute K -th order derivatives. It is possible to derive more “pedagogical” approaches, which however require hand-crafted interpolation rules case by case, and propagation of higher-order jets which is costly (see §E.2 for a pedagogical example using less efficient 6-jets to compute the biharmonic operator, or [27, §F] for other operators).

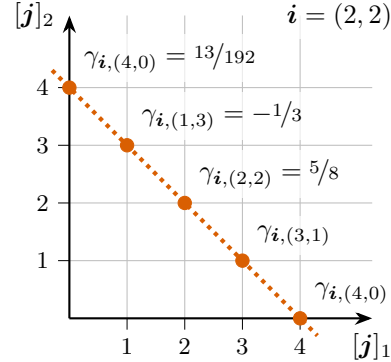


Figure 4: **Illustration of eq. (12) for the biharmonic operator**, i.e., the 5 values of j with $\|j\|_1 = 4$ and their coefficients $\gamma_{i,j}$ to interpolate the desired mixed partials.

4 Implementation & Experiments

Here, we describe our implementation of the Taylor mode collapsing process and empirically validate its performance improvements on the previously discussed operators.

Design decisions & limitations. JAX [3] already offers an—albeit experimental—Taylor mode implementation [2]. However, we found it challenging to capture the computation graph and modify it using JAX’s public interface. In contrast, PyTorch [22] provides `torch.fx` [26], which offers a user-friendly interface to capture and transform computational graphs purely in Python. Hence, we re-implemented Taylor mode in PyTorch, taking heavy inspiration from the JAX implementation.

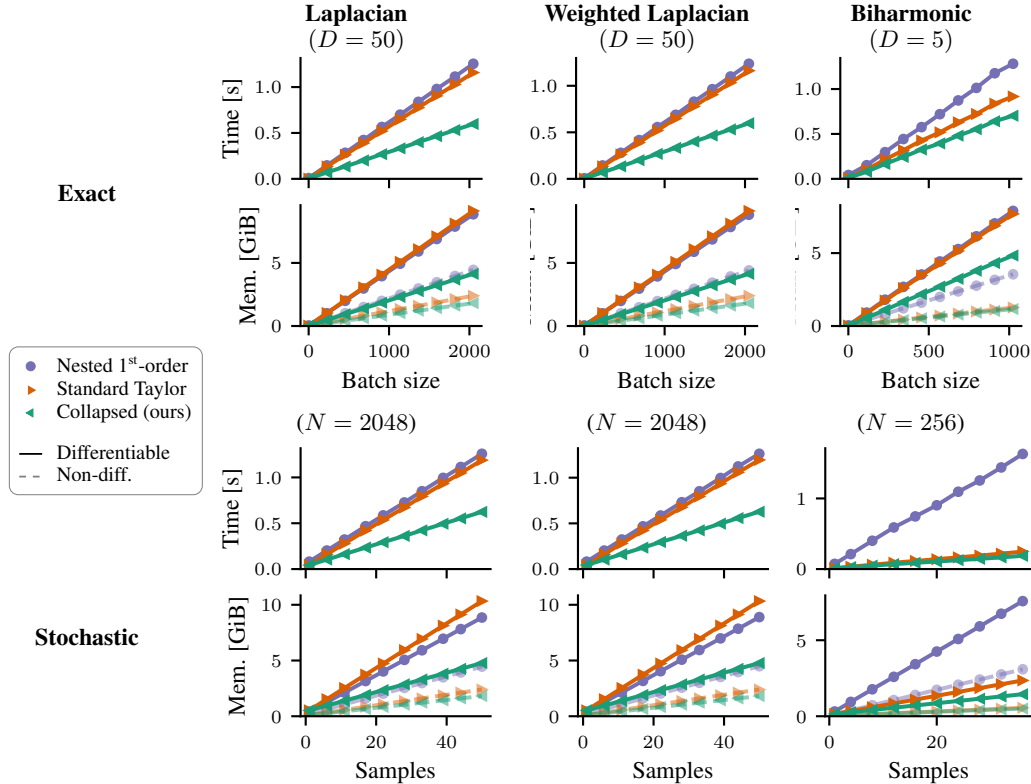


Figure 5: **Collapsed Taylor mode accelerates standard Taylor mode and outperforms nested 1st-order AD.** Exact computation varies the batch size, stochastic computation fixes a batch size and varies the samples such that $S < D$ (Laplacians), and $2 + 3S < 9/2D^2 - 3/2D + 4$ (biharmonic operator); we could compute exactly otherwise. Opaque markers are non-differentiable computations.

This deliberate choice imposes certain limitations. First, as of now, our Taylor mode in PyTorch supports only a small number of primitives, because the Taylor arithmetic in eq. (3) needs to be implemented case by case (this of course also applies to JAX’s Taylor mode, which has broader operator coverage). Second, while our Taylor mode implementation is competitive with JAX’s, we did not fully optimize it (e.g., we do *not* use in-place operations, and we do *not* implement the efficient schemes from Griewank & Walther [13, §13], but stick to Faà di Bruno (eq. (3))). Given our implementation’s superiority compared to nested first-order AD that we demonstrate below, these are promising future efforts that will further improve performance, and we believe that making Taylor mode available to the PyTorch community is also an important step towards establishing its use.

Usage (overview in §B). Our implementation takes a PyTorch function (e.g., a neural net) and first captures its computational graph using `torch.fx`’s symbolic tracing mechanism. Then, it replaces each operation with its Taylor arithmetic, which yields the computational graph of the function’s K -jet. Users can then write a function to compute their differential operator with this vanilla Taylor mode. Collapsing is achieved using a function `simplify`, which traces the computation again, rewrites the graph, and propagates the summation of highest coefficients up to its leafs. This requires one backward traversal through the graph (§C presents a detailed example). The simplified graph produces the same result, but propagates summed coefficients, i.e., uses collapsed Taylor mode.

Experimental setup. We empirically validate our proposed collapsing approach in PyTorch. We compare **standard Taylor mode** with **collapsed Taylor mode** and **nested 1st-order AD** on an Nvidia RTX 6000 GPU with 24 GiB memory. To implement the (weighted) Laplacian and its stochastic counterpart, we use vector-Hessian-vector products (VHVPs) in forward-over-reverse order, as recommended [5, 13]. For the biharmonic operator, we simply nest two VHVPs. For the weighted Laplacian’s coefficient matrix, we choose a full-rank diagonal matrix (§F.2 shows results for rank-

Table 1: **Benchmark from fig. 5 in numbers.** We fit linear functions and report their slopes, i.e., how much runtime and memory increase when incrementing the batch size or random samples. We show two significant digits and bold values are best according to parenthesized values.

| Mode | Per-datum or -sample cost | Implementation | Laplacian | Weighted Laplacian | Biharmonic |
|---------------------------|--------------------------------|-------------------------------|---------------------|---------------------|---------------------|
| Exact \times | Time [ms] | Nested 1 st -order | 0.61 (1.0x) | 0.60 (1.0x) | 1.2 (1.0x) |
| | | Standard Taylor | 0.56 (0.93x) | 0.57 (0.94x) | 0.90 (0.72x) |
| | | Collapsed (ours) | 0.29 (0.48x) | 0.29 (0.48x) | 0.69 (0.55x) |
| | Mem. [MiB] (differentiable) | Nested 1 st -order | 4.4 (1.0x) | 4.4 (1.0x) | 7.9 (1.0x) |
| | | Standard Taylor | 4.6 (1.0x) | 4.6 (1.0x) | 7.7 (0.98x) |
| | | Collapsed (ours) | 2.1 (0.47x) | 2.1 (0.47x) | 4.8 (0.61x) |
| Mem. [MiB] (non-diff.) | Nested 1 st -order | 2.2 (1.0x) | 2.2 (1.0x) | 3.5 (1.0x) | |
| | Standard Taylor | 1.2 (0.54x) | 1.2 (0.54x) | 1.2 (0.36x) | |
| | Collapsed (ours) | 0.90 (0.41x) | 0.90 (0.41x) | 1.1 (0.33x) | |
| Stochastic | Time [ms] | Nested 1 st -order | 24 (1.0x) | 24 (1.0x) | 44 (1.0x) |
| | | Standard Taylor | 23 (0.97x) | 23 (0.97x) | 6.6 (0.15x) |
| | | Collapsed (ours) | 12 (0.49x) | 12 (0.49x) | 4.9 (0.11x) |
| | Mem. [MiB] (differentiable) | Nested 1 st -order | 180 (1.0x) | 180 (1.0x) | 210 (1.0x) |
| | | Standard Taylor | 200 (1.2x) | 200 (1.2x) | 64 (0.30x) |
| | | Collapsed (ours) | 89 (0.50x) | 89 (0.50x) | 38 (0.18x) |
| Mem. [MiB] (non-diff.) | Nested 1 st -order | 89 (1.0x) | 90 (1.0x) | 86 (1.0x) | |
| | Standard Taylor | 48 (0.54x) | 48 (0.53x) | 15 (0.17x) | |
| | Collapsed (ours) | 36 (0.40x) | 36 (0.40x) | 13 (0.16x) | |

deficient weightings). To avoid confounding factors, all implementations are executed without compilation (our JAX experiments with the Laplacian in §G confirm that `jit` does not affect the relative performance). As common for PINNs [e.g., 6, 27], we use a 5-layer MLP $f_\theta : D \rightarrow 768 \rightarrow 768 \rightarrow 512 \rightarrow 512 \rightarrow 1$ with tanh activations and trainable parameters θ , and compute the PDE operators on batches of size N . We measure three performance metrics: **(1) runtime** reports the smallest execution time of 50 repetitions. **(2) Peak memory (non-differentiable)** measures the maximum allocated GPU memory when computing the PDE operator’s value (e.g., used in VMC [24]) inside a `torch.no_grad` context. **(3) Peak memory (differentiable)** is the maximum memory usage when computing the PDE operator inside a `torch.enable_grad` context, which allows backpropagation to θ (required for training PINNs, or alternative VMC works [30, 32]). This demands saving intermediates, which uses more memory but does not affect runtime. As memory allocation does not fluctuate much, we measure it in a single run.

Results. Figure 5 visualizes the growth in computational resources w.r.t. the batch size (exact) and random samples (stochastic) for fixed dimensions D . Runtime and memory increase linearly in both, as expected. We quantify the results by fitting linear functions and reporting their slopes (i.e., time and memory added per datum/sample) in table 1. We make the following observations:

- **Collapsed Taylor mode accelerates standard Taylor mode.** The measured performance differences correspond well with the theoretical estimate from counting the number of forward-propagated vectors. E.g., for the exact Laplacian, adding one datum introduces $2 + D$ versus $1 + 2D$ new vectors. For $D = 50$, their ratio is $(2+D)/(1+2D) \approx 0.51$. Empirically, we measure that adding one datum adds **0.56 ms** to standard, and **0.29 ms** to collapsed, Taylor mode (table 1); the ratio of ≈ 0.52 is close. Similar arguments hold for peak memory of differentiable computation, stochastic approximation, and the other PDE operators (see table F2 for all comparisons).
- **Collapsed Taylor mode outperforms nested 1st-order AD.** For the exact and stochastic (weighted) Laplacians, collapsed Taylor mode is roughly twice as fast (consistent with the JAX results in fig. 1) while using only 40-50% memory. For the biharmonic operator, we also observe speed-ups; in the stochastic case up to 9x in time, and 5x in memory (differentiable).

Comparison with JAX. We also conducted experiments with JAX (+ `jit`) to rule out artifacts from choosing PyTorch, implementation mistakes in our Taylor mode library, or unexpected simplifications from the JIT compiler. We find that the choice of the ML framework does not affect the results. E.g., when computing the exact Laplacian with nested first-order AD, PyTorch consumes 0.61 ms per datum (table 1), while JAX uses 0.58 ms (fig. 1 and table G5). We find the same trend when comparing our collapsed Taylor mode and JAX’s forward Laplacian. Interestingly, we noticed that JAX’s Taylor mode was consistently slower than our PyTorch implementation, despite using `jit`. We hypothesize that this could stem from algorithmic differences in the Taylor mode implementations and conclude from these results that (both ours, as well as the existing JAX) Taylor mode still has potential for improvements that may further increase the margin to nested first-order.

5 Conclusion

Computing differential operators is a critical component in scientific machine learning, particularly for Physics-informed neural networks and variational Monte-Carlo. Our work introduces collapsed Taylor mode, a simple yet effective optimization based on linearity in Faà di Bruno’s formula, that propagates the sum of highest-order Taylor coefficients, rather than propagating then summing. It contains recent advances in forward-mode schemes, recovering the forward Laplacian [21], while being applicable to stochastic Taylor mode [17, 27]. We demonstrated that collapsed Taylor mode is useful to compute general linear differential operators, leveraging Griewank et al. [14]’s interpolation formula. Empirically, we confirmed speed-ups and memory savings for computing (randomized) Laplacians and biharmonic operators after collapsing Taylor mode, in accordance with our theoretical analysis, and confirmed its superiority to nesting first-order automatic differentiation. As the optimizations are achieved through simple graph rewrites based on linearity, we believe they could be integrated into existing just-in-time compilers without requiring a new interface or burdening users.

Our work takes an important step towards making Taylor mode a practical alternative to nested first-order differentiation in scientific machine learning, while maintaining ease of use. Future work could focus on integrating these optimizations directly into ML compilers, broadening operator coverage of our PyTorch implementation, and exploring additional graph optimizations for AD.

Acknowledgments and Disclosure of Funding

Resources used in preparing this research were provided, in part, by the Province of Ontario, the Government of Canada through CIFAR, and companies sponsoring the Vector Institute. The research was funded partly by the DFG under Germany’s Excellence Strategy – The Berlin Mathematics Research Center MATH+ (EXC-2046/1, project ID:390685689). M.Z. acknowledges support from an ETH Postdoctoral Fellowship for the project “Reliable, Efficient, and Scalable Methods for Scientific Machine Learning”.

References

- [1] Arbogast, L. *Du calcul des dérivations*. 1800.
- [2] Bettencourt, J., Johnson, M. J., and Duvenaud, D. Taylor-mode automatic differentiation for higher-order derivatives in JAX. In *Advances in Neural Information Processing Systems (NeurIPS); Workshop on Program Transformations for ML*, 2019.
- [3] Bradbury, J., Frostig, R., Hawkins, P., Johnson, M. J., Leary, C., Maclaurin, D., and Wanderman-Milne, S. JAX: composable transformations of Python+NumPy programs, 2018.
- [4] Carleo, G. and Troyer, M. Solving the quantum many-body problem with artificial neural networks. *Science*, 355(6325):602–606, 2017.
- [5] Dagréou, M., Ablin, P., Vaiter, S., and Moreau, T. How to compute Hessian-vector products? In *International Conference on Learning Representations (ICLR) Blogposts*, 2024.
- [6] Dangel, F., Müller, J., and Zeinhofer, M. Kronecker-factored approximate curvature for physics-informed neural networks. In *Advances in Neural Information Processing Systems (NeurIPS)*, 2024.

- [7] Dwivedi, V. and Srinivasan, B. Solution of biharmonic equation in complicated geometries with physics informed extreme learning machine. *Journal of Computing and Information Science in Engineering*, 20(6), 05 2020. ISSN 1530-9827.
- [8] Fa, K. S. Solution of Fokker-Planck equation for a broad class of drift and diffusion coefficients. *Phys. Rev. E*, 2011.
- [9] Faà Di Bruno, F. Note sur une nouvelle formule de calcul différentiel. *Quarterly J. Pure Appl. Math*, 1857.
- [10] Foulkes, W. M., Mitas, L., Needs, R., and Rajagopal, G. Quantum Monte Carlo simulations of solids. *Reviews of Modern Physics*, 73(1):33, 2001.
- [11] Fraenkel, L. Formulae for high derivatives of composite functions. In *Mathematical Proceedings of the Cambridge Philosophical Society*, 1978.
- [12] Gao, N., Köhler, J., and Foster, A. folx - forward Laplacian for JAX, 2023. URL <http://github.com/microsoft/folx>.
- [13] Griewank, A. and Walther, A. *Evaluating derivatives: principles and techniques of algorithmic differentiation*. SIAM, 2008.
- [14] Griewank, A., Utke, J., and Walther, A. Evaluating higher derivative tensors by forward propagation of univariate Taylor series. *Mathematics of Computation*, 69, 1999.
- [15] Hardy, M. Combinatorics of partial derivatives, 2006. arXiv.
- [16] Hermann, J., Schätzle, Z., and Noé, F. Deep-neural-network solution of the electronic Schrödinger equation. *Nature Chemistry*, 12(10):891–897, 2020.
- [17] Hu, Z., Shi, Z., Karniadakis, G. E., and Kawaguchi, K. Hutchinson trace estimation for high-dimensional and high-order physics-informed neural networks. *Computer Methods in Applied Mechanics and Engineering*, 2024.
- [18] Hutchinson, M. A stochastic estimator of the trace of the influence matrix for laplacian smoothing splines. *Communication in Statistics—Simulation and Computation*, 1989.
- [19] Karniadakis, G. E., Kevrekidis, I. G., Lu, L., Perdikaris, P., Wang, S., and Yang, L. Physics-informed machine learning. *Nature Reviews Physics*, 3(6):422–440, 2021.
- [20] Li, R., Wang, C., Ye, H., He, D., and Wang, L. DOF: Accelerating high-order differential operators with forward propagation. In *International Conference on Learning Representations (ICLR), Workshop on AI4DifferentialEquations In Science*, 2024.
- [21] Li, R., Ye, H., Jiang, D., Wen, X., Wang, C., Li, Z., Li, X., He, D., Chen, J., Ren, W., et al. A computational framework for neural network-based variational Monte Carlo with forward Laplacian. *Nature Machine Intelligence*, 2024.
- [22] Paszke, A., Gross, S., Massa, F., Lerer, A., Bradbury, J., Chanan, G., Killeen, T., Lin, Z., Gimelshein, N., Antiga, L., Desmaison, A., Kopf, A., Yang, E., DeVito, Z., Raison, M., Tejani, A., Chilamkurthy, S., Steiner, B., Fang, L., Bai, J., and Chintala, S. PyTorch: An imperative style, high-performance deep learning library. In *Advances in Neural Information Processing Systems (NeurIPS)*. 2019.
- [23] Pearlmutter, B. A. Fast exact multiplication by the Hessian. *Neural Computation*, 1994.
- [24] Pfau, D., Spencer, J. S., Matthews, A. G., and Foulkes, W. M. C. Ab initio solution of the many-electron Schrödinger equation with deep neural networks. *Physical Review Research*, 2020.
- [25] Raissi, M., Perdikaris, P., and Karniadakis, G. E. Physics-informed neural networks: A deep learning framework for solving forward and inverse problems involving nonlinear partial differential equations. *Journal of Computational physics*, 378:686–707, 2019.

- [26] Reed, J., DeVito, Z., He, H., Ussery, A., and Ansel, J. torch.fx: Practical program capture and transformation for deep learning in python. *Proceedings of Machine Learning and Systems (MLSys)*, 2022.
- [27] Shi, Z., Hu, Z., Lin, M., and Kawaguchi, K. Stochastic Taylor derivative estimator: Efficient amortization for arbitrary differential operators. In *Advances in Neural Information Processing Systems (NeurIPS)*, 2024.
- [28] Sun, J., Berner, J., Richter, L., Zeinhofer, M., Müller, J., Azizzadenesheli, K., and Anandkumar, A. Dynamical measure transport and neural PDE solvers for sampling. *arXiv preprint arXiv:2407.07873*, 2024.
- [29] Sun, R., Li, D., Liang, S., Ding, T., and Srikant, R. The global landscape of neural networks: An overview, 2020.
- [30] Toulouse, J. and Umrigar, C. J. Optimization of quantum Monte Carlo wave functions by energy minimization. *The Journal of Chemical Physics (JCP)*, 2007.
- [31] Vahab, M., Haghghat, E., Khaleghi, M., and Khalili, N. A physics-informed neural network approach to solution and identification of biharmonic equations of elasticity. *Journal of Engineering Mechanics*, 148(2), 2022.
- [32] Webber, R. J. and Lindsey, M. Rayleigh-Gauss-Newton optimization with enhanced sampling for variational Monte Carlo. *Physical Review Research*, 2022.

NeurIPS Paper Checklist

1. Claims

Question: Do the main claims made in the abstract and introduction accurately reflect the paper's contributions and scope?

Answer: [Yes]

Justification: We propose an acceleration technique for Taylor mode automatic differentiation (AD), describe the scope of its applicability and how it works, then empirically verify the claimed acceleration capabilities. This is clearly communicated in the abstract.

Guidelines:

- The answer NA means that the abstract and introduction do not include the claims made in the paper.
- The abstract and/or introduction should clearly state the claims made, including the contributions made in the paper and important assumptions and limitations. A No or NA answer to this question will not be perceived well by the reviewers.
- The claims made should match theoretical and experimental results, and reflect how much the results can be expected to generalize to other settings.
- It is fine to include aspirational goals as motivation as long as it is clear that these goals are not attained by the paper.

2. Limitations

Question: Does the paper discuss the limitations of the work performed by the authors?

Answer: [Yes]

Justification: We specifically incorporate a paragraph about limitations of the implementation in §4 and state the assumptions (linear differential operator) under which the proposed optimization technique is applicable.

Guidelines:

- The answer NA means that the paper has no limitation while the answer No means that the paper has limitations, but those are not discussed in the paper.
- The authors are encouraged to create a separate "Limitations" section in their paper.
- The paper should point out any strong assumptions and how robust the results are to violations of these assumptions (e.g., independence assumptions, noiseless settings, model well-specification, asymptotic approximations only holding locally). The authors should reflect on how these assumptions might be violated in practice and what the implications would be.
- The authors should reflect on the scope of the claims made, e.g., if the approach was only tested on a few datasets or with a few runs. In general, empirical results often depend on implicit assumptions, which should be articulated.
- The authors should reflect on the factors that influence the performance of the approach. For example, a facial recognition algorithm may perform poorly when image resolution is low or images are taken in low lighting. Or a speech-to-text system might not be used reliably to provide closed captions for online lectures because it fails to handle technical jargon.
- The authors should discuss the computational efficiency of the proposed algorithms and how they scale with dataset size.
- If applicable, the authors should discuss possible limitations of their approach to address problems of privacy and fairness.
- While the authors might fear that complete honesty about limitations might be used by reviewers as grounds for rejection, a worse outcome might be that reviewers discover limitations that aren't acknowledged in the paper. The authors should use their best judgment and recognize that individual actions in favor of transparency play an important role in developing norms that preserve the integrity of the community. Reviewers will be specifically instructed to not penalize honesty concerning limitations.

3. Theory assumptions and proofs

Question: For each theoretical result, does the paper provide the full set of assumptions and a complete (and correct) proof?

Answer: [NA]

Justification: The paper does not present new theoretical results. All theoretical results used in this work (specifically, [14]) are cited, and we include self-contained introductions that are relevant to our approach in the appendix (specifically, §E).

Guidelines:

- The answer NA means that the paper does not include theoretical results.
- All the theorems, formulas, and proofs in the paper should be numbered and cross-referenced.
- All assumptions should be clearly stated or referenced in the statement of any theorems.
- The proofs can either appear in the main paper or the supplemental material, but if they appear in the supplemental material, the authors are encouraged to provide a short proof sketch to provide intuition.
- Inversely, any informal proof provided in the core of the paper should be complemented by formal proofs provided in appendix or supplemental material.
- Theorems and Lemmas that the proof relies upon should be properly referenced.

4. Experimental result reproducibility

Question: Does the paper fully disclose all the information needed to reproduce the main experimental results of the paper to the extent that it affects the main claims and/or conclusions of the paper (regardless of whether the code and data are provided or not)?

Answer: [Yes]

Justification: We describe the experimental procedure, including hardware and hyperparameter details, in §4, together with a more detailed description in §F and G, where we also partially reproduce our results using a different ML library. We will open-source the code used to produce our results to further facilitate their reproducibility.

Guidelines:

- The answer NA means that the paper does not include experiments.
- If the paper includes experiments, a No answer to this question will not be perceived well by the reviewers: Making the paper reproducible is important, regardless of whether the code and data are provided or not.
- If the contribution is a dataset and/or model, the authors should describe the steps taken to make their results reproducible or verifiable.
- Depending on the contribution, reproducibility can be accomplished in various ways. For example, if the contribution is a novel architecture, describing the architecture fully might suffice, or if the contribution is a specific model and empirical evaluation, it may be necessary to either make it possible for others to replicate the model with the same dataset, or provide access to the model. In general, releasing code and data is often one good way to accomplish this, but reproducibility can also be provided via detailed instructions for how to replicate the results, access to a hosted model (e.g., in the case of a large language model), releasing of a model checkpoint, or other means that are appropriate to the research performed.
- While NeurIPS does not require releasing code, the conference does require all submissions to provide some reasonable avenue for reproducibility, which may depend on the nature of the contribution. For example
 - (a) If the contribution is primarily a new algorithm, the paper should make it clear how to reproduce that algorithm.
 - (b) If the contribution is primarily a new model architecture, the paper should describe the architecture clearly and fully.
 - (c) If the contribution is a new model (e.g., a large language model), then there should either be a way to access this model for reproducing the results or a way to reproduce the model (e.g., with an open-source dataset or instructions for how to construct the dataset).

- (d) We recognize that reproducibility may be tricky in some cases, in which case authors are welcome to describe the particular way they provide for reproducibility. In the case of closed-source models, it may be that access to the model is limited in some way (e.g., to registered users), but it should be possible for other researchers to have some path to reproducing or verifying the results.

5. Open access to data and code

Question: Does the paper provide open access to the data and code, with sufficient instructions to faithfully reproduce the main experimental results, as described in supplemental material?

Answer: [Yes]

Justification: We will open-source the code for our PyTorch Taylor mode library (which is not the main contribution of our paper), as well as the code used to generate our results, including instructions how to reproduce them. See the link in the main text.

Guidelines:

- The answer NA means that paper does not include experiments requiring code.
- Please see the NeurIPS code and data submission guidelines (<https://nips.cc/public/guides/CodeSubmissionPolicy>) for more details.
- While we encourage the release of code and data, we understand that this might not be possible, so “No” is an acceptable answer. Papers cannot be rejected simply for not including code, unless this is central to the contribution (e.g., for a new open-source benchmark).
- The instructions should contain the exact command and environment needed to run to reproduce the results. See the NeurIPS code and data submission guidelines (<https://nips.cc/public/guides/CodeSubmissionPolicy>) for more details.
- The authors should provide instructions on data access and preparation, including how to access the raw data, preprocessed data, intermediate data, and generated data, etc.
- The authors should provide scripts to reproduce all experimental results for the new proposed method and baselines. If only a subset of experiments are reproducible, they should state which ones are omitted from the script and why.
- At submission time, to preserve anonymity, the authors should release anonymized versions (if applicable).
- Providing as much information as possible in supplemental material (appended to the paper) is recommended, but including URLs to data and code is permitted.

6. Experimental setting/details

Question: Does the paper specify all the training and test details (e.g., data splits, hyper-parameters, how they were chosen, type of optimizer, etc.) necessary to understand the results?

Answer: [Yes]

Justification: Our experiments consist of performance measurements. We clearly specify the protocol, used hardware, architectural details, and other hyper-parameters in §4, with more details in §F and G.

Guidelines:

- The answer NA means that the paper does not include experiments.
- The experimental setting should be presented in the core of the paper to a level of detail that is necessary to appreciate the results and make sense of them.
- The full details can be provided either with the code, in appendix, or as supplemental material.

7. Experiment statistical significance

Question: Does the paper report error bars suitably and correctly defined or other appropriate information about the statistical significance of the experiments?

Answer: [Yes]

Justification: While we do not report error bars, we choose the experimental procedure to minimize noise: To measure runtime, we report the smallest number from repeating a run 50 times. Reporting mean and standard deviations is less conclusive because runtimes on hardware can vary due to interference from other processes or warm-up effects during the first execution. Reporting the minimum time as best approximation to the actual runtime is recommended, e.g. in <https://realpython.com/python-profiling/>.

Guidelines:

- The answer NA means that the paper does not include experiments.
- The authors should answer "Yes" if the results are accompanied by error bars, confidence intervals, or statistical significance tests, at least for the experiments that support the main claims of the paper.
- The factors of variability that the error bars are capturing should be clearly stated (for example, train/test split, initialization, random drawing of some parameter, or overall run with given experimental conditions).
- The method for calculating the error bars should be explained (closed form formula, call to a library function, bootstrap, etc.)
- The assumptions made should be given (e.g., Normally distributed errors).
- It should be clear whether the error bar is the standard deviation or the standard error of the mean.
- It is OK to report 1-sigma error bars, but one should state it. The authors should preferably report a 2-sigma error bar than state that they have a 96% CI, if the hypothesis of Normality of errors is not verified.
- For asymmetric distributions, the authors should be careful not to show in tables or figures symmetric error bars that would yield results that are out of range (e.g. negative error rates).
- If error bars are reported in tables or plots, The authors should explain in the text how they were calculated and reference the corresponding figures or tables in the text.

8. Experiments compute resources

Question: For each experiment, does the paper provide sufficient information on the computer resources (type of compute workers, memory, time of execution) needed to reproduce the experiments?

Answer: [Yes]

Justification: We mention the exact type of GPU used in §4. Since we evaluate runtime and memory performances, we used a single GPU. The total compute time can be estimated by multiplying our reported timings with the number of repetitions, then summing over all measurement points. It totals less than 24 GPU hours.

Guidelines:

- The answer NA means that the paper does not include experiments.
- The paper should indicate the type of compute workers CPU or GPU, internal cluster, or cloud provider, including relevant memory and storage.
- The paper should provide the amount of compute required for each of the individual experimental runs as well as estimate the total compute.
- The paper should disclose whether the full research project required more compute than the experiments reported in the paper (e.g., preliminary or failed experiments that didn't make it into the paper).

9. Code of ethics

Question: Does the research conducted in the paper conform, in every respect, with the NeurIPS Code of Ethics <https://neurips.cc/public/EthicsGuidelines?>

Answer: [Yes]

Justification: After carefully reading the Code of Ethics, we believe our research conforms with it.

Guidelines:

- The answer NA means that the authors have not reviewed the NeurIPS Code of Ethics.
- If the authors answer No, they should explain the special circumstances that require a deviation from the Code of Ethics.
- The authors should make sure to preserve anonymity (e.g., if there is a special consideration due to laws or regulations in their jurisdiction).

10. Broader impacts

Question: Does the paper discuss both potential positive societal impacts and negative societal impacts of the work performed?

Answer: [NA]

Justification: Our work introduces algorithmic improvements to Taylor mode automatic differentiation. We think they positively impact the research landscape of scientific machine learning, by reducing computational resources. We do not foresee any direct negative societal impacts of our work.

Guidelines:

- The answer NA means that there is no societal impact of the work performed.
- If the authors answer NA or No, they should explain why their work has no societal impact or why the paper does not address societal impact.
- Examples of negative societal impacts include potential malicious or unintended uses (e.g., disinformation, generating fake profiles, surveillance), fairness considerations (e.g., deployment of technologies that could make decisions that unfairly impact specific groups), privacy considerations, and security considerations.
- The conference expects that many papers will be foundational research and not tied to particular applications, let alone deployments. However, if there is a direct path to any negative applications, the authors should point it out. For example, it is legitimate to point out that an improvement in the quality of generative models could be used to generate deepfakes for disinformation. On the other hand, it is not needed to point out that a generic algorithm for optimizing neural networks could enable people to train models that generate Deepfakes faster.
- The authors should consider possible harms that could arise when the technology is being used as intended and functioning correctly, harms that could arise when the technology is being used as intended but gives incorrect results, and harms following from (intentional or unintentional) misuse of the technology.
- If there are negative societal impacts, the authors could also discuss possible mitigation strategies (e.g., gated release of models, providing defenses in addition to attacks, mechanisms for monitoring misuse, mechanisms to monitor how a system learns from feedback over time, improving the efficiency and accessibility of ML).

11. Safeguards

Question: Does the paper describe safeguards that have been put in place for responsible release of data or models that have a high risk for misuse (e.g., pretrained language models, image generators, or scraped datasets)?

Answer: [NA]

Justification: Our work neither uses data sets, nor trains models.

Guidelines:

- The answer NA means that the paper poses no such risks.
- Released models that have a high risk for misuse or dual-use should be released with necessary safeguards to allow for controlled use of the model, for example by requiring that users adhere to usage guidelines or restrictions to access the model or implementing safety filters.
- Datasets that have been scraped from the Internet could pose safety risks. The authors should describe how they avoided releasing unsafe images.
- We recognize that providing effective safeguards is challenging, and many papers do not require this, but we encourage authors to take this into account and make a best faith effort.

12. Licenses for existing assets

Question: Are the creators or original owners of assets (e.g., code, data, models), used in the paper, properly credited and are the license and terms of use explicitly mentioned and properly respected?

Answer: [Yes]

Justification: We give credit to code packages we use through citations, specifically JAX's Taylor mode [2] and forward Laplacian [12], as well as `torch.fx` [26].

Guidelines:

- The answer NA means that the paper does not use existing assets.
- The authors should cite the original paper that produced the code package or dataset.
- The authors should state which version of the asset is used and, if possible, include a URL.
- The name of the license (e.g., CC-BY 4.0) should be included for each asset.
- For scraped data from a particular source (e.g., website), the copyright and terms of service of that source should be provided.
- If assets are released, the license, copyright information, and terms of use in the package should be provided. For popular datasets, paperswithcode.com/datasets has curated licenses for some datasets. Their licensing guide can help determine the license of a dataset.
- For existing datasets that are re-packaged, both the original license and the license of the derived asset (if it has changed) should be provided.
- If this information is not available online, the authors are encouraged to reach out to the asset's creators.

13. New assets

Question: Are new assets introduced in the paper well documented and is the documentation provided alongside the assets?

Answer: [Yes]

Justification: Our PyTorch implementation of Taylor mode is fully-documented and tested. We are planning to open-source it soon.

Guidelines:

- The answer NA means that the paper does not release new assets.
- Researchers should communicate the details of the dataset/code/model as part of their submissions via structured templates. This includes details about training, license, limitations, etc.
- The paper should discuss whether and how consent was obtained from people whose asset is used.
- At submission time, remember to anonymize your assets (if applicable). You can either create an anonymized URL or include an anonymized zip file.

14. Crowdsourcing and research with human subjects

Question: For crowdsourcing experiments and research with human subjects, does the paper include the full text of instructions given to participants and screenshots, if applicable, as well as details about compensation (if any)?

Answer: [NA]

Justification: The paper does not involve crowdsourcing nor research with human subjects.

Guidelines:

- The answer NA means that the paper does not involve crowdsourcing nor research with human subjects.
- Including this information in the supplemental material is fine, but if the main contribution of the paper involves human subjects, then as much detail as possible should be included in the main paper.

- According to the NeurIPS Code of Ethics, workers involved in data collection, curation, or other labor should be paid at least the minimum wage in the country of the data collector.

15. Institutional review board (IRB) approvals or equivalent for research with human subjects

Question: Does the paper describe potential risks incurred by study participants, whether such risks were disclosed to the subjects, and whether Institutional Review Board (IRB) approvals (or an equivalent approval/review based on the requirements of your country or institution) were obtained?

Answer: [NA]

Justification: The paper does not involve crowdsourcing nor research with human subjects.

Guidelines:

- The answer NA means that the paper does not involve crowdsourcing nor research with human subjects.
- Depending on the country in which research is conducted, IRB approval (or equivalent) may be required for any human subjects research. If you obtained IRB approval, you should clearly state this in the paper.
- We recognize that the procedures for this may vary significantly between institutions and locations, and we expect authors to adhere to the NeurIPS Code of Ethics and the guidelines for their institution.
- For initial submissions, do not include any information that would break anonymity (if applicable), such as the institution conducting the review.

16. Declaration of LLM usage

Question: Does the paper describe the usage of LLMs if it is an important, original, or non-standard component of the core methods in this research? Note that if the LLM is used only for writing, editing, or formatting purposes and does not impact the core methodology, scientific rigor, or originality of the research, declaration is not required.

Answer: [NA]

Justification: Our work does not rely on LLM usage in any way.

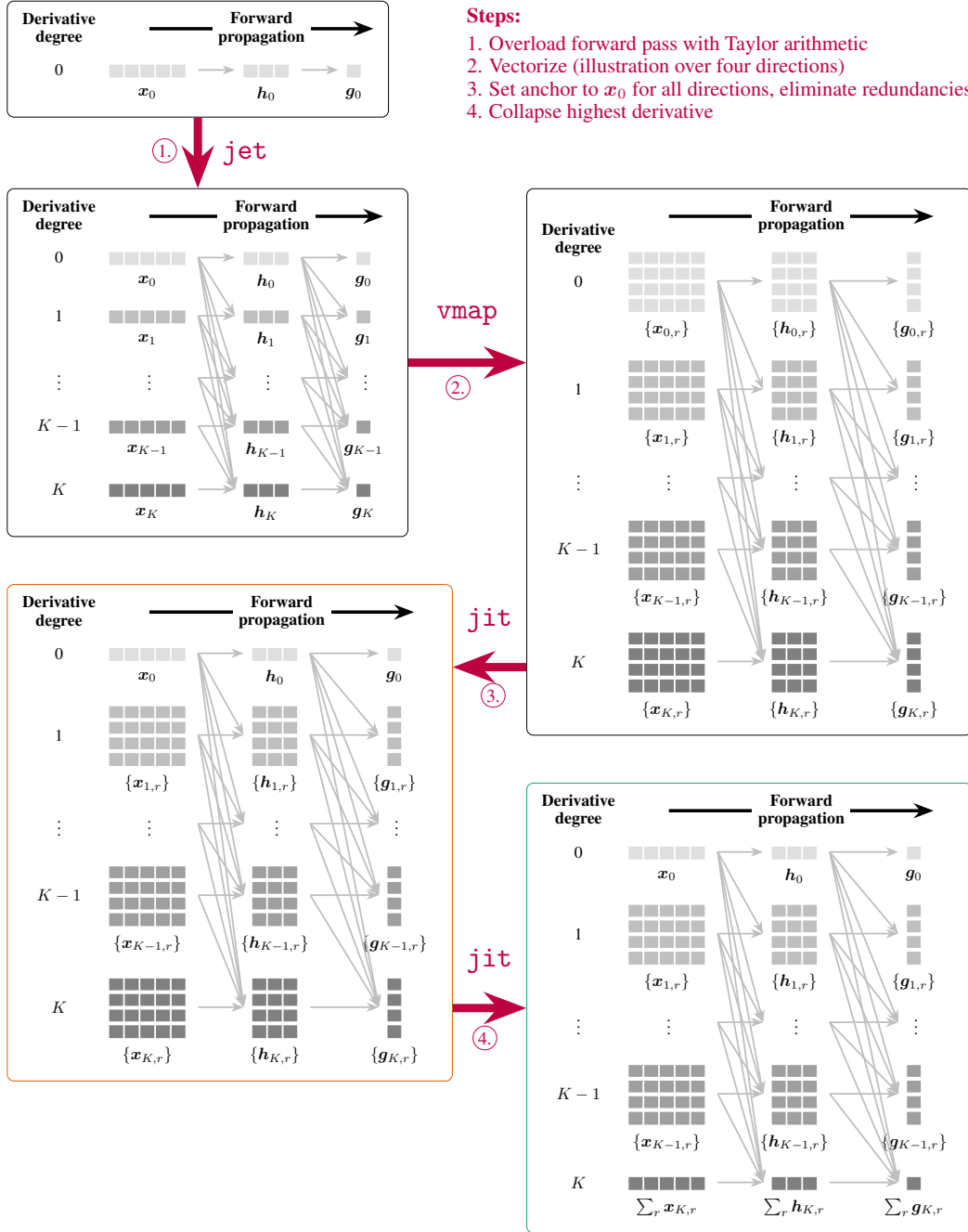
Guidelines:

- The answer NA means that the core method development in this research does not involve LLMs as any important, original, or non-standard components.
- Please refer to our LLM policy (<https://neurips.cc/Conferences/2025/LLM>) for what should or should not be described.

Collapsing Taylor Mode Automatic Differentiation (Supplementary Material)

| | | |
|----------|---|-----------|
| A | Faà Di Bruno Formula Cheat Sheet | 21 |
| B | Visual Tour: From Function to Collapsed Taylor Mode | 22 |
| C | Graph Simplifications | 23 |
| D | Exploiting Linearity to Collapse Taylor Mode | 26 |
| | D.1 Second-order Operators: Laplacian | 27 |
| E | (Collapsed) Taylor Mode for Arbitrary Mixed Partial Derivatives | 28 |
| | E.1 Applied to the Biharmonic Operator | 29 |
| | E.2 Pedagogical Approach for the Biharmonic Operator with 6-jets | 30 |
| | E.3 Another Example: Mixed Third-order Derivatives | 31 |
| F | PyTorch Benchmark | 32 |
| | F.1 Additional Analysis and Impact of <code>torch.compile</code> | 32 |
| | F.2 Rank-deficient Weighted Laplacian | 34 |
| G | JAX Benchmark | 34 |
| H | Numerical Complexity and Error Analysis | 37 |
| I | Connections of Collapsed Taylor Mode to Existing Methods | 39 |
| | I.1 Connection to Randomized Laplacian via Hutchinson’s Trace Estimator | 39 |
| | I.2 Connection to the Forward Laplacian | 40 |

B Visual Tour: From Function to Collapsed Taylor Mode



Steps:

1. Overload forward pass with Taylor arithmetic
2. Vectorize (illustration over four directions)
3. Set anchor to x_0 for all directions, eliminate redundancies
4. Collapse highest derivative

Figure B6: **Step-by-step transformation of a function into its collapsed Taylor mode.** Collapsed Taylor mode can be implemented via the already existing `jet` (standard Taylor mode), `vmap` (vectorization), and `jit` (graph transformation) interfaces. Therefore, users do not need to learn a new interface to benefit from our proposed method and can simply rely on standard Taylor mode and just-in-time compilation (after incorporating our proposed simplifications). Coloured boxes correspond to our PyTorch implementations of **standard** and **collapsed** Taylor mode from our experiments.

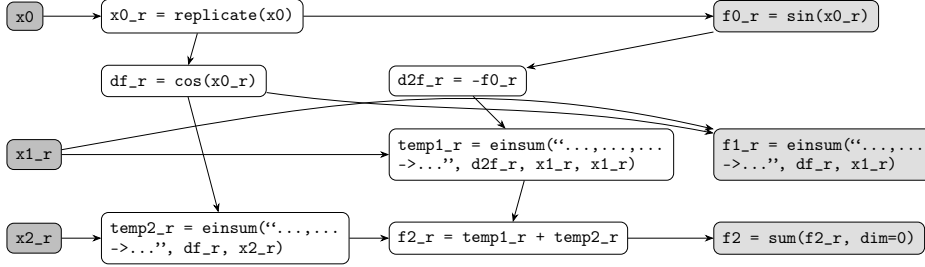
C Graph Simplifications

In this section, we illustrate the two graph simplifications that are required to collapse Taylor mode.

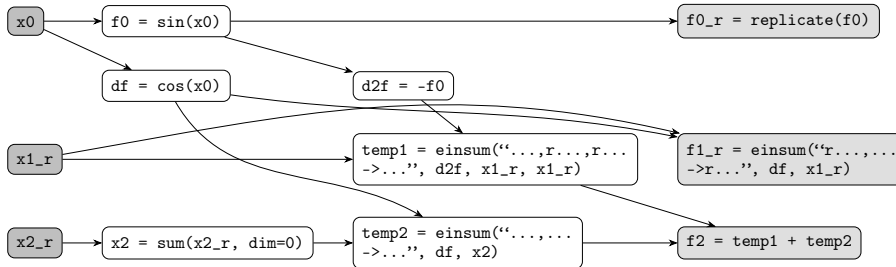
We will consider collapsing the 2-jet of $f = \sin$ as an example. Recall the propagation scheme eq. (D13) and assume that the Taylor coefficients are given by $\{x_{0,r} = x_0\}$, $\{x_{1,r}\}$, and $\{x_{2,r}\}$ where r indexes the directions along which we evaluate the sum:

$$\begin{aligned} \begin{matrix} x_0 \\ \{x_{1,r}\} \\ \{x_{2,r}\} \end{matrix} &\xrightarrow{\text{replicate } x_0} \begin{matrix} x_{0,r} = x_0 \\ x_{1,r} \\ x_{2,r} \end{matrix} \xrightarrow{\text{(D13)}} \begin{matrix} f_{0,r} = \sin(x_0) \\ f_{1,r} = \cos(x_0) \odot x_{1,r} \\ f_{2,r} = -\sin(x_0) \odot x_{1,r} \odot x_{1,r} + \cos(x_0) \odot x_{2,r} \end{matrix} \\ &\xrightarrow{\text{sum highest component}} \begin{matrix} f_{0,r} \\ f_{1,r} \\ \sum_r f_{2,r} \end{matrix} \end{aligned}$$

Here, \sin applies element-wise and \odot denotes element-wise multiplication. The computational graph for this procedure is displayed in the following diagram, with input and output nodes highlighted in dark and light gray. The suffix $_r$ means that all R corresponding tensors are stacked along their leading axis. `replicate` is a function that replicates a tensor R times along a new leading axis, which is in PyTorch usually for free and without additional memory overhead (using `torch.expand`). All other functions refer to those of the PyTorch API:



Our simplification proceeds in two steps. First, propagate `replicate` nodes down the graph to remove repeated computations on the same tensors. This is done in a forward traversal through the graph. Second, in a single backward traversal through the graph, we propagate the `sum` node up. After applying both steps, the graph looks as follows:



Two important properties of the new graph are (i) the `replicate` node moved to an output node, hence the corresponding redundant computation was successfully removed (ii) the highest component $x_{2,r}$ is immediately summed then propagated, i.e., we collapsed Taylor mode and avoid the separate propagation for all $x_{2,r}$.

We will now illustrate the two simplification steps in full detail. The first stage starts from the original graph and pushes forward the `replicate` node, as illustrated step-by-step in fig. C7. The second stage starts from the graph produced by the `replicate`-push procedure, and propagates the final `sum` node up the graph, illustrated by fig. C8. This yields the final computation graph shown above.

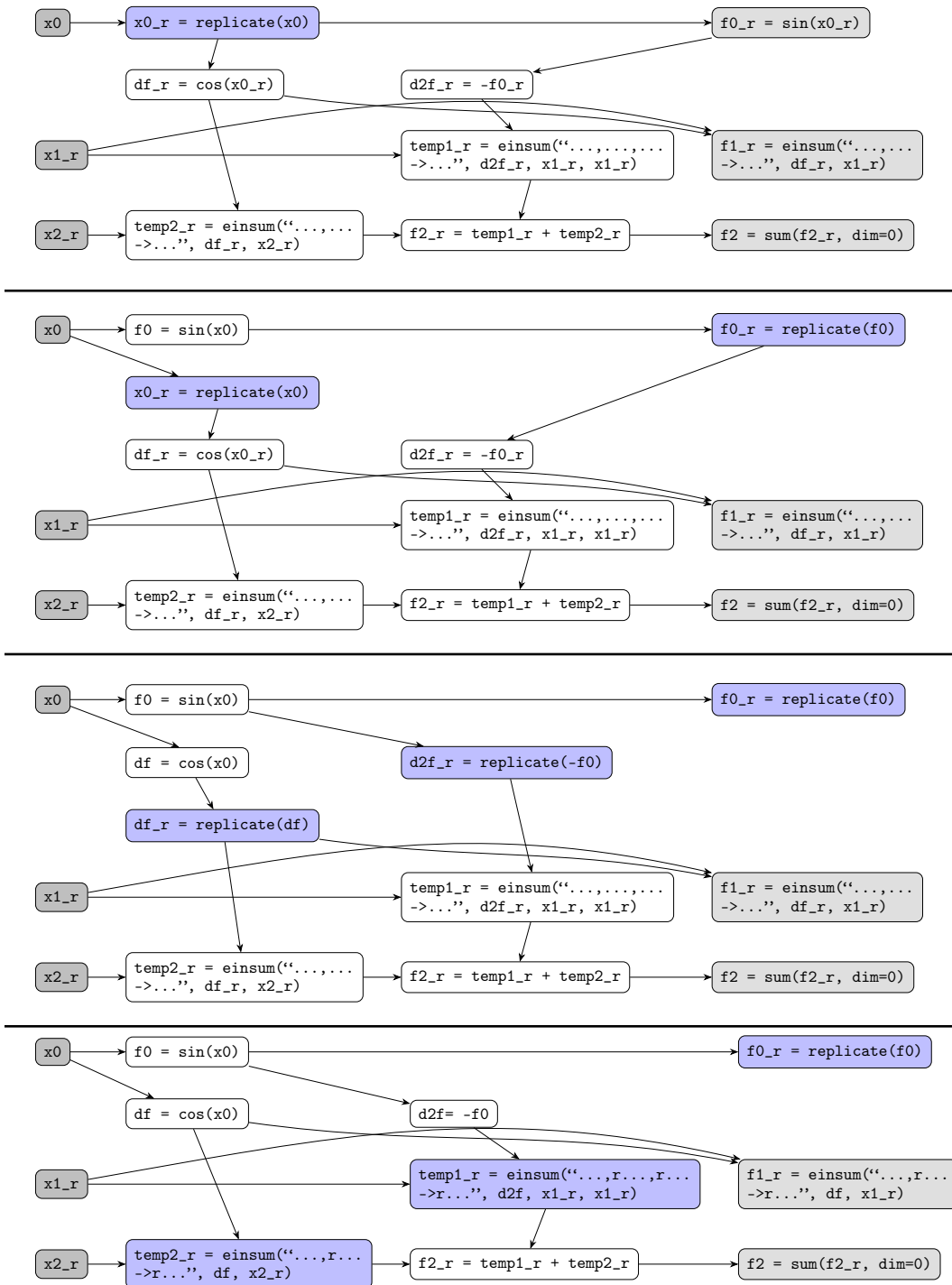


Figure C7: Step-by-step illustration of pushing replicate nodes down a computation graph.

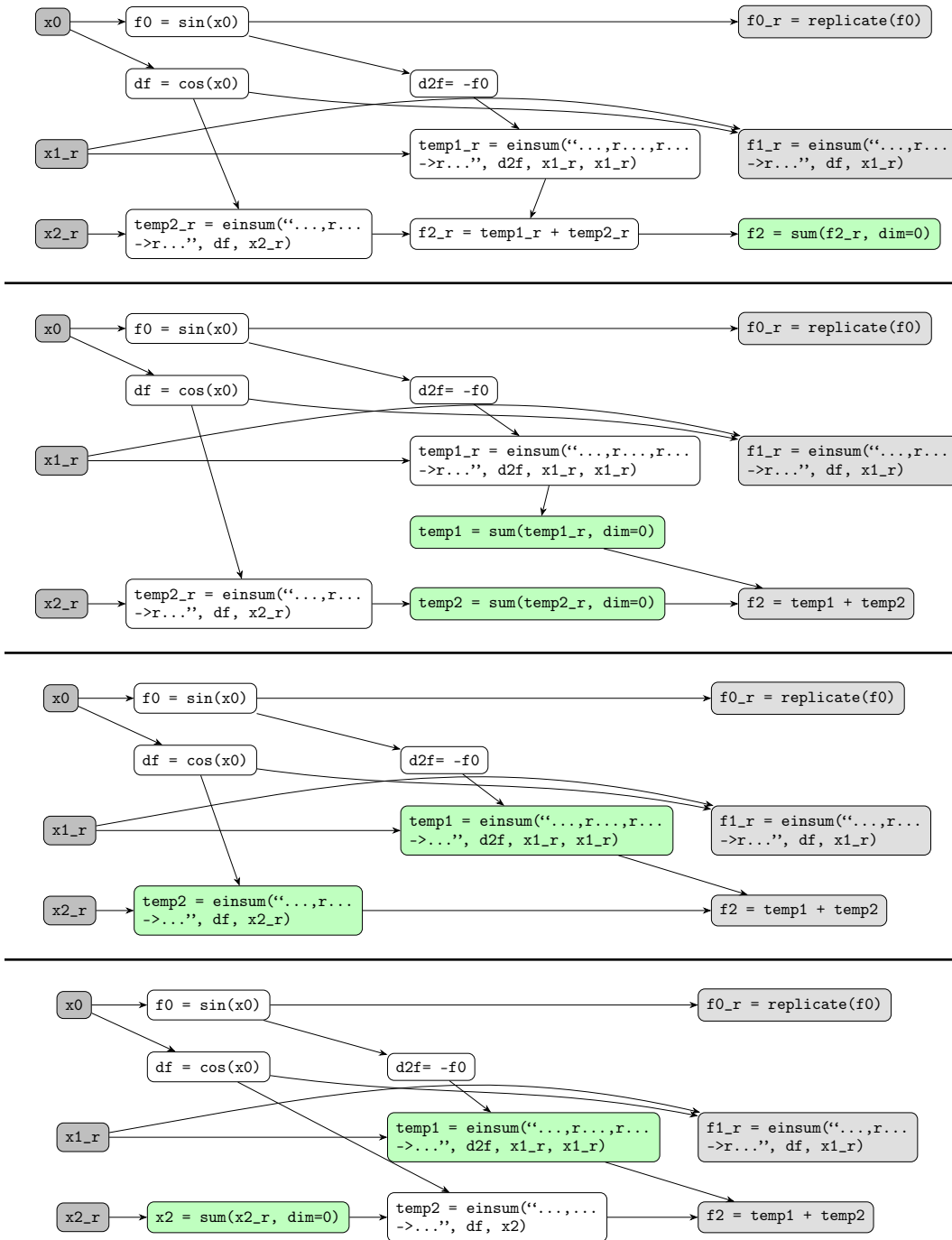


Figure C8: Step-by-step illustration of propagating sum nodes up a computation graph.

D Exploiting Linearity to Collapse Taylor Mode

Here, we illustrate the idea behind propagating R K -jets through $\mathbf{f} = \mathbf{g} \circ \mathbf{h}$ with input jets $(J^K \mathbf{x})_r(t) = \sum_{k=0}^K \frac{t^k}{k!} \mathbf{x}_{k,r}$. The Taylor mode scheme results from inserting eq. (5) into eq. (4):

$$\begin{aligned}
& \begin{pmatrix} \mathbf{x}_0 \\ \{\mathbf{x}_{1,r}\} \\ \{\mathbf{x}_{2,r}\} \\ \vdots \\ \{\mathbf{x}_{K,r}\} \end{pmatrix} \stackrel{(3)}{\rightarrow} \begin{pmatrix} \mathbf{h}_0 = \mathbf{h}(\mathbf{x}_0) \\ \{\mathbf{h}_{1,r}\} = \{\langle \partial \mathbf{h}(\mathbf{x}_0), \mathbf{x}_{1,r} \rangle\} \\ \{\mathbf{h}_{2,r}\} = \{\langle \partial^2 \mathbf{h}(\mathbf{x}_0), \mathbf{x}_{1,r} \otimes \mathbf{x}_{1,r} \rangle + \langle \partial \mathbf{h}(\mathbf{x}_0), \mathbf{x}_{2,r} \rangle\} \\ \vdots \\ \{\mathbf{h}_{K,r}\} = \left\{ \sum_{\sigma \in \text{part}(K)} \nu(\sigma) \left\langle \partial^{|\sigma|} \mathbf{h}(\mathbf{x}_0), \otimes_{s \in \sigma} \mathbf{x}_{s,r} \right\rangle \right\} \end{pmatrix} \\
& \stackrel{(3)}{\rightarrow} \begin{pmatrix} \mathbf{g}_0 = \mathbf{g}(\mathbf{h}_0) \\ \{\mathbf{g}_{1,r}\} = \{\langle \partial \mathbf{g}(\mathbf{h}_0), \mathbf{h}_{1,r} \rangle\} \\ \{\mathbf{g}_{2,r}\} = \{\langle \partial^2 \mathbf{g}(\mathbf{h}_0), \mathbf{h}_{1,r} \otimes \mathbf{h}_{1,r} \rangle + \langle \partial \mathbf{g}(\mathbf{h}_0), \mathbf{h}_{2,r} \rangle\} \\ \vdots \\ \{\mathbf{g}_{K,r}\} = \left\{ \sum_{\sigma \in \text{part}(K)} \nu(\sigma) \left\langle \partial^{|\sigma|} \mathbf{g}(\mathbf{h}_0), \otimes_{s \in \sigma} \mathbf{h}_{s,r} \right\rangle \right\} \end{pmatrix} \quad (\text{D13}) \\
& \stackrel{(3)}{=} \begin{pmatrix} \mathbf{f}_0 = \mathbf{f}(\mathbf{x}_0) \\ \{\mathbf{f}_{1,r}\} = \{\langle \partial \mathbf{f}(\mathbf{x}_0), \mathbf{x}_{1,r} \rangle\} \\ \{\mathbf{f}_{2,r}\} = \{\langle \partial^2 \mathbf{f}(\mathbf{x}_0), \mathbf{x}_{1,r} \otimes \mathbf{x}_{1,r} \rangle + \langle \partial \mathbf{f}(\mathbf{x}_0), \mathbf{x}_{2,r} \rangle\} \\ \vdots \\ \{\mathbf{f}_{K,r}\} = \left\{ \sum_{\sigma \in \text{part}(K)} \nu(\sigma) \left\langle \partial^{|\sigma|} \mathbf{f}(\mathbf{x}_0), \otimes_{s \in \sigma} \mathbf{x}_{s,r} \right\rangle \right\} \end{pmatrix} \\
& \xrightarrow{\text{slice}} \{\mathbf{g}_{K,r}\} \\
& \xrightarrow{\text{sum}} \sum_{r=1}^R \mathbf{g}_{K,r} \big|_{\{\mathbf{x}_{1,r}=\mathbf{v}_r, \mathbf{x}_{2,r}=\dots=\mathbf{x}_{K,r}=\mathbf{0}\}} \sum_{r=1}^R \langle \partial^K \mathbf{f}(\mathbf{x}_0), \otimes_{k=1}^K \mathbf{v}_r \rangle
\end{aligned}$$

Leveraging linearity in certain terms (in green) of the highest coefficient, as explained in eq. (6), instead leads to

$$\begin{aligned}
& \begin{pmatrix} \mathbf{x}_0 \\ \{\mathbf{x}_{1,r}\} \\ \{\mathbf{x}_{2,r}\} \\ \vdots \\ \sum_{r=1}^R \mathbf{x}_{K,r} \end{pmatrix} \stackrel{(3)}{\rightarrow} \begin{pmatrix} \mathbf{h}_0 = \mathbf{h}(\mathbf{x}_0) \\ \{\mathbf{h}_{1,r}\} = \{\langle \partial \mathbf{h}(\mathbf{x}_0), \mathbf{x}_{1,r} \rangle\} \\ \{\mathbf{h}_{2,r}\} = \{\langle \partial^2 \mathbf{h}(\mathbf{x}_0), \mathbf{x}_{1,r} \otimes \mathbf{x}_{1,r} \rangle + \langle \partial \mathbf{h}(\mathbf{x}_0), \mathbf{x}_{2,r} \rangle\} \\ \vdots \\ \sum_{r=1}^R \mathbf{h}_{K,r} = \sum_{r=1}^R \sum_{\sigma \in \text{part}(K) \setminus \{\bar{\sigma}\}} \nu(\sigma) \left\langle \partial^{|\sigma|} \mathbf{h}(\mathbf{x}_0), \otimes_{s \in \sigma} \mathbf{x}_{s,r} \right\rangle \\ + \left\langle \partial \mathbf{h}(\mathbf{x}_0), \sum_{r=1}^R \mathbf{x}_{K,r} \right\rangle \end{pmatrix} \\
& \stackrel{(3)}{\rightarrow} \begin{pmatrix} \mathbf{g}_0 = \mathbf{g}(\mathbf{h}_0) \\ \{\mathbf{g}_{1,r}\} = \{\langle \partial \mathbf{g}(\mathbf{h}_0), \mathbf{h}_{1,r} \rangle\} \\ \{\mathbf{g}_{2,r}\} = \{\langle \partial^2 \mathbf{g}(\mathbf{h}_0), \mathbf{h}_{1,r} \otimes \mathbf{h}_{1,r} \rangle + \langle \partial \mathbf{g}(\mathbf{h}_0), \mathbf{h}_{2,r} \rangle\} \\ \vdots \\ \sum_{r=1}^R \mathbf{g}_{K,r} = \sum_{r=1}^R \sum_{\sigma \in \text{part}(K) \setminus \{\bar{\sigma}\}} \nu(\sigma) \left\langle \partial^{|\sigma|} \mathbf{g}(\mathbf{h}_0), \otimes_{s \in \sigma} \mathbf{h}_{s,r} \right\rangle \\ + \left\langle \partial \mathbf{g}(\mathbf{h}_0), \sum_{r=1}^R \mathbf{h}_{K,r} \right\rangle \end{pmatrix} \quad (\text{D14})
\end{aligned}$$

$$\begin{aligned}
& \begin{pmatrix} \mathbf{f}_0 & = & \mathbf{f}(\mathbf{x}_0) \\ \{\mathbf{f}_{1,r}\} & = & \{\langle \partial \mathbf{f}(\mathbf{x}_0), \mathbf{x}_{1,r} \rangle\} \\ \{\mathbf{f}_{2,r}\} & = & \{\langle \partial^2 \mathbf{f}(\mathbf{x}_0), \mathbf{x}_{1,r} \otimes \mathbf{x}_{1,r} \rangle + \langle \partial \mathbf{f}(\mathbf{x}_0), \mathbf{x}_{2,r} \rangle\} \\ \vdots & & \\ \sum_{r=1}^R \mathbf{f}_{K,r} & = & \sum_{r=1}^R \sum_{\sigma \in \text{part}(K) \setminus \{\bar{\sigma}\}} \nu(\sigma) \left\langle \partial^{|\sigma|} \mathbf{f}(\mathbf{x}_0), \otimes_{s \in \sigma} \mathbf{x}_{s,r} \right\rangle \\ & & + \left\langle \partial \mathbf{f}(\mathbf{x}_0), \sum_{r=1}^R \mathbf{x}_{K,r} \right\rangle \end{pmatrix} \\
& \xrightarrow{\text{slice}} \sum_{r=1}^R \mathbf{g}_{K,r} \quad \{\mathbf{x}_{1,r} = \mathbf{v}_r, \mathbf{x}_{2,r} = \dots = \mathbf{x}_{K,r} = \mathbf{0}\} \sum_{r=1}^R \langle \partial^K \mathbf{f}(\mathbf{x}_0), \otimes_{k=1}^K \mathbf{v}_r \rangle
\end{aligned}$$

D.1 Second-order Operators: Laplacian

Here, we show details about the propagation schemes of standard Taylor mode and collapsed Taylor mode for the computation of the Laplacian of \mathbf{f} . We consider the decomposition $\mathbf{f} = \mathbf{g} \circ \mathbf{h}$.

Standard Taylor mode. Using standard Taylor mode (eq. (D13)) to compute the Laplacian yields

$$\begin{aligned}
& \begin{pmatrix} \mathbf{x}_0 \\ \{\mathbf{x}_{1,d}\} \\ \{\mathbf{x}_{2,d}\} \end{pmatrix} \xrightarrow{(3)} \begin{pmatrix} \mathbf{h}_0 = \mathbf{h}(\mathbf{x}_0) \\ \{\mathbf{h}_{1,d}\} = \{\langle \partial \mathbf{h}(\mathbf{x}_0), \mathbf{x}_{1,d} \rangle\} \\ \{\mathbf{h}_{2,d}\} = \{\langle \partial^2 \mathbf{h}(\mathbf{x}_0), \mathbf{x}_{1,d} \otimes \mathbf{x}_{1,d} \rangle + \langle \partial \mathbf{h}(\mathbf{x}_0), \mathbf{x}_{2,d} \rangle\} \end{pmatrix} \\
& \xrightarrow{(3)} \begin{pmatrix} \mathbf{g}_0 = \mathbf{g}(\mathbf{h}_0) \\ \{\mathbf{g}_{1,d}\} = \{\langle \partial \mathbf{g}(\mathbf{h}_0), \mathbf{h}_{1,d} \rangle\} \\ \{\mathbf{g}_{2,d}\} = \{\langle \partial^2 \mathbf{g}(\mathbf{h}_0), \mathbf{h}_{1,d} \otimes \mathbf{h}_{1,d} \rangle + \langle \partial \mathbf{g}(\mathbf{h}_0), \mathbf{h}_{2,d} \rangle\} \end{pmatrix} \\
& \xrightarrow{(3)} \begin{pmatrix} \mathbf{f}_0 = \mathbf{f}(\mathbf{x}_0) \\ \{\mathbf{f}_{1,d}\} = \{\langle \partial \mathbf{f}(\mathbf{x}_0), \mathbf{x}_{1,d} \rangle\} \\ \{\mathbf{f}_{2,d}\} = \{\langle \partial^2 \mathbf{f}(\mathbf{x}_0), \mathbf{x}_{1,d} \otimes \mathbf{x}_{1,d} \rangle + \langle \partial \mathbf{f}(\mathbf{x}_0), \mathbf{x}_{2,d} \rangle\} \end{pmatrix} \tag{D15} \\
& \xrightarrow{\text{slice}} \{\mathbf{g}_{2,d}\} \\
& \xrightarrow{\text{sum}} \sum_{d=1}^D \{\mathbf{g}_{2,d}\} \quad \{\mathbf{x}_{1,d} = \mathbf{e}_d, \mathbf{x}_{2,d} = \mathbf{0}\} \Delta \mathbf{f}(\mathbf{x}_0).
\end{aligned}$$

Collapsed Taylor Mode AD Using our proposed collapsed Taylor mode, we get

$$\begin{aligned}
& \begin{pmatrix} \mathbf{x}_0 \\ \{\mathbf{x}_{1,d}\} \\ \sum_{d=1}^D \mathbf{x}_{2,d} \end{pmatrix} \xrightarrow{(1)} \begin{pmatrix} \mathbf{h}_0 = \mathbf{h}(\mathbf{x}_0) \\ \{\mathbf{h}_{1,d}\} = \{\langle \partial \mathbf{h}(\mathbf{x}_0), \mathbf{x}_{1,d} \rangle\} \\ \sum_{d=1}^D \mathbf{h}_{2,d} = \sum_{d=1}^D \langle \partial^2 \mathbf{h}(\mathbf{x}_0), \mathbf{x}_{1,d} \otimes \mathbf{x}_{1,d} \rangle + \left\langle \partial \mathbf{h}(\mathbf{x}_0), \sum_{d=1}^D \mathbf{x}_{2,d} \right\rangle \end{pmatrix} \\
& \xrightarrow{(1)} \begin{pmatrix} \mathbf{g}_0 = \mathbf{g}(\mathbf{h}_0) \\ \{\mathbf{g}_{1,d}\} = \{\langle \partial \mathbf{g}(\mathbf{h}_0), \mathbf{h}_{1,d} \rangle\} \\ \sum_{d=1}^D \mathbf{g}_{2,d} = \sum_{d=1}^D \langle \partial^2 \mathbf{g}(\mathbf{h}_0), \mathbf{h}_{1,d} \otimes \mathbf{h}_{1,d} \rangle + \left\langle \partial \mathbf{g}(\mathbf{h}_0), \sum_{d=1}^D \mathbf{h}_{2,d} \right\rangle \end{pmatrix} \tag{D16} \\
& \xrightarrow{(1)} \begin{pmatrix} \mathbf{f}_0 = \mathbf{f}(\mathbf{x}_0) \\ \{\mathbf{f}_{1,d}\} = \{\langle \partial \mathbf{f}(\mathbf{x}_0), \mathbf{x}_{1,d} \rangle\} \\ \sum_{d=1}^D \mathbf{f}_{2,d} = \sum_{d=1}^D \langle \partial^2 \mathbf{f}(\mathbf{x}_0), \mathbf{x}_{1,d} \otimes \mathbf{x}_{1,d} \rangle + \left\langle \partial \mathbf{f}(\mathbf{x}_0), \sum_{i=1}^D \mathbf{x}_{2,d} \right\rangle \end{pmatrix} \\
& \xrightarrow{\text{slice}} \sum_{d=1}^D \{\mathbf{g}_{2,d}\} \quad \{\mathbf{x}_{1,d} = \mathbf{e}_d, \mathbf{x}_{2,d} = \mathbf{0}\} \Delta \mathbf{f}(\mathbf{x}_0)
\end{aligned}$$

E (Collapsed) Taylor Mode for Arbitrary Mixed Partial Derivatives

Here, we introduce the notation of eq. (11). The right side of the formula sums over the set of all $\mathbf{j} \in \mathbb{N}^I$ such that $\|\mathbf{j}\|_1 := \sum_i [j]_i = K$. For example, if $I = 2$ and $\|\mathbf{j}\|_1 = 4$, this set is $\{(4, 0), (0, 4), (3, 1), (1, 3), (2, 2)\}$.

The coefficient $\gamma_{i,j}$ is defined as

$$\gamma_{i,j} := \sum_{0 < \mathbf{m} \leq \mathbf{i}} (-1)^{\|\mathbf{i}-\mathbf{m}\|_1} \binom{\mathbf{i}}{\mathbf{m}} \binom{\|\mathbf{i}\|_1 \frac{\mathbf{m}}{\|\mathbf{m}\|_1}}{\mathbf{j}} \left(\frac{\|\mathbf{m}\|_1}{\|\mathbf{i}\|_1} \right)^{\|\mathbf{i}\|_1}. \quad (\text{E17})$$

The summation ranges over the set $\{\mathbf{m} \in \mathbb{N}^I \mid [\mathbf{m}]_1 \leq [\mathbf{i}]_1, \dots, [\mathbf{m}]_I \leq [\mathbf{i}]_I, \|\mathbf{m}\|_1 > 0\}$. Furthermore, we utilize the generalized binomial coefficient

$$\binom{a}{b} := \prod_{l=0}^{b-1} \frac{a-l}{b-l}$$

to allow the computation for all $a \in \mathbb{R}$ and $b \in \mathbb{N}$, which is defined to be 1 if $b = 0$. The generalized binomial coefficient of vectors is the component-wise product of generalized binomial coefficients:

$$\binom{\mathbf{a}}{\mathbf{b}} := \prod_{i=1}^I \binom{[\mathbf{a}]_i}{[\mathbf{b}]_i}.$$

This notation also includes cases where the vector \mathbf{a} has components of \mathbb{R} .

Example computation. Let us compute the coefficient $\gamma_{(2,2),(3,1)}$, used by the biharmonic operator:

$$\gamma_{(2,2),(3,1)} = \sum_{\substack{\mathbf{m} \in \mathbb{N}, \|\mathbf{m}\|_1 > 0 \\ [\mathbf{m}]_1 \leq 2, [\mathbf{m}]_2 \leq 2}} (-1)^{2-[\mathbf{m}]_1+2-[\mathbf{m}]_2} \binom{2}{[\mathbf{m}]_1} \binom{2}{[\mathbf{m}]_2} \binom{4 \frac{[\mathbf{m}]_1}{\|\mathbf{m}\|_1}}{3} \binom{4 \frac{[\mathbf{m}]_2}{\|\mathbf{m}\|_1}}{1} \left(\frac{\|\mathbf{m}\|_1}{4} \right)^4.$$

We have $\mathbf{m} \in \{(1, 0), (2, 0), (1, 1), (2, 1), (2, 2), (1, 2), (0, 1), (0, 2)\}$, which results in the terms

$$\begin{aligned} &= (-1)^{2-1+2-0} \binom{2}{1} \binom{2}{0} \binom{4 \frac{1}{3}}{3} \binom{4 \frac{0}{1}}{1} \left(\frac{1}{4} \right)^4 \\ &+ (-1)^{2-2+2-0} \binom{2}{2} \binom{2}{0} \binom{4 \frac{2}{3}}{3} \binom{4 \frac{0}{1}}{1} \left(\frac{2}{4} \right)^4 \\ &+ (-1)^{2-1+2-1} \binom{2}{1} \binom{2}{1} \binom{4 \frac{1}{2}}{3} \binom{4 \frac{1}{1}}{1} \left(\frac{2}{4} \right)^4 \\ &+ (-1)^{2-2+2-1} \binom{2}{2} \binom{2}{1} \binom{4 \frac{2}{3}}{3} \binom{4 \frac{1}{1}}{1} \left(\frac{3}{4} \right)^4 \\ &+ (-1)^{2-2+2-2} \binom{2}{2} \binom{2}{2} \binom{4 \frac{2}{4}}{3} \binom{4 \frac{2}{1}}{1} \left(\frac{4}{4} \right)^4 \\ &+ (-1)^{2-1+2-2} \binom{2}{1} \binom{2}{2} \binom{4 \frac{1}{3}}{3} \binom{4 \frac{2}{1}}{1} \left(\frac{3}{4} \right)^4 \\ &+ (-1)^{2-0+2-1} \binom{2}{0} \binom{2}{1} \binom{4 \frac{0}{3}}{3} \binom{4 \frac{1}{1}}{1} \left(\frac{1}{4} \right)^4 \\ &+ (-1)^{2-0+2-2} \binom{2}{0} \binom{2}{2} \binom{4 \frac{0}{3}}{3} \binom{4 \frac{2}{1}}{1} \left(\frac{2}{4} \right)^4. \end{aligned}$$

The next step is to evaluate the binomial coefficients:

$$\begin{aligned}
&= (-1) \cdot 2 \cdot 1 \cdot 4 \cdot 0 \cdot \left(\frac{1}{4}\right)^4 \\
&\quad + 1 \cdot 1 \cdot 4 \cdot 0 \cdot \left(\frac{2}{4}\right)^4 \\
&\quad + 2 \cdot 2 \cdot 0 \cdot 2 \cdot \left(\frac{2}{4}\right)^4 \\
&\quad - 1 \cdot 2 \cdot \frac{8}{9} \frac{5}{6} \frac{2}{3} \cdot \frac{4}{3} \cdot \left(\frac{3}{4}\right)^4 \\
&\quad + 1 \cdot 1 \cdot 0 \cdot 2 \cdot \left(\frac{4}{4}\right)^4 \\
&\quad - 2 \cdot 1 \cdot \frac{4}{9} \frac{1}{6} \frac{-2}{3} \cdot \frac{8}{3} \cdot \left(\frac{3}{4}\right)^4 \\
&\quad - 1 \cdot 2 \cdot 0 \cdot 4 \cdot \left(\frac{1}{4}\right)^4 \\
&\quad + 1 \cdot 1 \cdot 1 \cdot 0 \cdot 4 \cdot \left(\frac{2}{4}\right)^4.
\end{aligned}$$

After simplification, the final result is

$$\begin{aligned}
\gamma_{(2,2),(3,1)} &= (-1) \cdot 2 \cdot \frac{8}{9} \frac{5}{6} \frac{2}{3} \cdot \frac{4}{3} \cdot \left(\frac{3}{4}\right)^4 - 2 \left(\frac{4}{9} \cdot \frac{1}{6} \cdot \frac{-2}{3}\right) \cdot \frac{8}{3} \cdot \left(\frac{3}{4}\right)^4 \\
&= \frac{-640}{486} \frac{81}{256} + \frac{128}{486} \frac{81}{256} = \frac{-5}{12} + \frac{1}{12} = -\frac{1}{3}.
\end{aligned}$$

E.1 Applied to the Biharmonic Operator

To compute eq. (9) with eq. (11), we first select $K = 4, I = 2, D_1 = D_2 = D, \mathbf{i} = (2, 2), \mathbf{v}_{d_1} = \mathbf{e}_{d_1}$ and $\mathbf{e}_{d_2} = \mathbf{e}_{d_2}$. Then we insert these parameters into the general equation eq. (11) and get

$$\begin{aligned}
\Delta^2 \mathbf{f}(\mathbf{x}_0) &= \sum_{\mathbf{j} \in \mathbb{N}^2, \|\mathbf{j}\|_1=4} \gamma_{(2,2),\mathbf{j}} \frac{1}{4!} \sum_{d_1=1}^D \sum_{d_2=1}^D \left\langle \partial^4 \mathbf{f}(\mathbf{x}_0), (\mathbf{e}_{d_1}[\mathbf{j}]_1 + \mathbf{e}_{d_2}[\mathbf{j}]_2)^{\otimes 4} \right\rangle \\
&= \frac{1}{24} \left(\gamma_{(2,2),(4,0)} \sum_{d_1=1}^D \sum_{d_2=1}^D \left\langle \partial^4 \mathbf{f}(\mathbf{x}_0), (4\mathbf{e}_{d_1})^{\otimes 4} \right\rangle \right. \\
&\quad + \gamma_{(2,2),(0,4)} \sum_{d_1=1}^D \sum_{d_2=1}^D \left\langle \partial^4 \mathbf{f}(\mathbf{x}_0), (4\mathbf{e}_{d_2})^{\otimes 4} \right\rangle \\
&\quad + \gamma_{(2,2),(3,1)} \sum_{d_1=1}^D \sum_{d_2=1}^D \left\langle \partial^4 \mathbf{f}(\mathbf{x}_0), (3\mathbf{e}_{d_1} + \mathbf{e}_{d_2})^{\otimes 4} \right\rangle \\
&\quad + \gamma_{(2,2),(1,3)} \sum_{d_1=1}^D \sum_{d_2=1}^D \left\langle \partial^4 \mathbf{f}(\mathbf{x}_0), (\mathbf{e}_{d_1} + 3\mathbf{e}_{d_2})^{\otimes 4} \right\rangle \\
&\quad \left. + \gamma_{(2,2),(2,2)} \sum_{d_1=1}^D \sum_{d_2=1}^D \left\langle \partial^4 \mathbf{f}(\mathbf{x}_0), (2\mathbf{e}_{d_1} + 2\mathbf{e}_{d_2})^{\otimes 4} \right\rangle \right). \tag{E18}
\end{aligned}$$

Now, exploit the symmetry of the coefficients $\gamma_{(2,2),(4,0)} = \gamma_{(2,2),(0,4)}$ and $\gamma_{(2,2),(3,1)} = \gamma_{(2,2),(1,3)}$ and the corresponding tensor basis expansion:

$$\begin{aligned}
&= \frac{1}{24} \left(2D\gamma_{(2,2),(4,0)} \sum_{d_1=1}^D \left\langle \partial^4 \mathbf{f}(\mathbf{x}_0), (4\mathbf{e}_{d_1})^{\otimes 4} \right\rangle \right. \\
&+ 2\gamma_{(2,2),(3,1)} \sum_{d_1=1}^D \sum_{d_2=1}^D \left\langle \partial^4 \mathbf{f}(\mathbf{x}_0), (3\mathbf{e}_{d_1} + \mathbf{e}_{d_2})^{\otimes 4} \right\rangle \\
&\left. + \gamma_{(2,2),(2,2)} \sum_{d_1=1}^D \sum_{d_2=1}^D \left\langle \partial^4 \mathbf{f}(\mathbf{x}_0), (2\mathbf{e}_{d_1} + 2\mathbf{e}_{d_2})^{\otimes 4} \right\rangle \right). \tag{E19}
\end{aligned}$$

Since the first sum captures all diagonal directions $\mathbf{e}_{d_1} = \mathbf{e}_{d_2}$, we extract this from the second and third sums to further reduce the computational effort:

$$\begin{aligned}
&= \frac{1}{24} \left((2D\gamma_{(2,2),(4,0)} + 2\gamma_{(2,2),(3,1)} + \gamma_{(2,2),(2,2)}) \sum_{d_1=1}^D \left\langle \partial^4 \mathbf{f}(\mathbf{x}_0), (4\mathbf{e}_{d_1})^{\otimes 4} \right\rangle \right. \\
&+ 2\gamma_{(2,2),(3,1)} \sum_{d_1=1}^D \sum_{\substack{d_2=1 \\ d_2 \neq d_1}}^D \left\langle \partial^4 \mathbf{f}(\mathbf{x}_0), (3\mathbf{e}_{d_1} + \mathbf{e}_{d_2})^{\otimes 4} \right\rangle \\
&\left. + \gamma_{(2,2),(2,2)} \sum_{d_1=1}^D \sum_{\substack{d_2=1 \\ d_2 \neq d_1}}^D \left\langle \partial^4 \mathbf{f}(\mathbf{x}_0), (2\mathbf{e}_{d_1} + 2\mathbf{e}_{d_2})^{\otimes 4} \right\rangle \right). \tag{E20}
\end{aligned}$$

Exploiting further symmetries in the last term's summation, we obtain

$$\begin{aligned}
\Delta^2 \mathbf{f}(\mathbf{x}_0) &= \frac{1}{24} \left((2D\gamma_{(2,2),(4,0)} + 2\gamma_{(2,2),(3,1)} + \gamma_{(2,2),(2,2)}) \sum_{d_1=1}^D \left\langle \partial^4 \mathbf{f}(\mathbf{x}_0), (4\mathbf{e}_{d_1})^{\otimes 4} \right\rangle \right. \\
&+ 2\gamma_{(2,2),(3,1)} \sum_{d_1=1}^D \sum_{\substack{d_2=1 \\ d_2 \neq d_1}}^D \left\langle \partial^4 \mathbf{f}(\mathbf{x}_0), (3\mathbf{e}_{d_1} + \mathbf{e}_{d_2})^{\otimes 4} \right\rangle \\
&\left. + 2\gamma_{(2,2),(2,2)} \sum_{d_1=1}^{D-1} \sum_{d_2=d_1+1}^D \left\langle \partial^4 \mathbf{f}(\mathbf{x}_0), (2\mathbf{e}_{d_1} + 2\mathbf{e}_{d_2})^{\otimes 4} \right\rangle \right). \tag{E21}
\end{aligned}$$

E.2 Pedagogical Approach for the Biharmonic Operator with 6-jets

A different approach to compute arbitrary-mixed derivatives was proposed in [27]. This approach relies, for the biharmonic operator, on the hand-selection of certain 6-jets to extract the required derivatives. The degree and directions for the jets are obtained by considering the Faà di Bruno formula for the 6-th coefficient \mathbf{f}_6 (see §A). Selecting coefficients of the input 6-jet to $\mathbf{x}_1 = \mathbf{e}_{d_1}$, $\mathbf{x}_2 = \mathbf{e}_{d_2}$ and $\mathbf{x}_3 = \mathbf{x}_4 = \mathbf{x}_5 = \mathbf{x}_6 = \mathbf{0}$ leads us to

$$\begin{aligned}
\mathbf{f}_6 &= \langle \partial^6 \mathbf{f}(\mathbf{x}_0), \mathbf{e}_{d_1}^{\otimes 6} \rangle + 15 \langle \partial^5 \mathbf{f}(\mathbf{x}_0), \mathbf{e}_{d_1}^{\otimes 4} \otimes \mathbf{e}_{d_2} \rangle \\
&+ 45 \langle \partial^4 \mathbf{f}(\mathbf{x}_0), \mathbf{e}_{d_1}^{\otimes 2} \otimes \mathbf{e}_{d_2}^{\otimes 2} \rangle + 15 \langle \partial^3 \mathbf{f}(\mathbf{x}_0), \mathbf{e}_{d_2}^{\otimes 3} \rangle. \tag{E22}
\end{aligned}$$

Notice the **blue term**, which has the same structure as the summands we want to compute for the biharmonic operator. Therefore, a first 6-jet is computed as explained above. To cancel out the unwanted terms, we evaluate another 6-jet with the same input except $\mathbf{x}_2 = -\mathbf{e}_{d_2}$ and adding the 6-th coefficient of this jet to eq. (E22) gives

$$2 \langle \partial^6 \mathbf{f}(\mathbf{x}_0), \mathbf{e}_{d_1}^{\otimes 6} \rangle + 90 \langle \partial^4 \mathbf{f}(\mathbf{x}_0), \mathbf{e}_{d_1}^{\otimes 2} \otimes \mathbf{e}_{d_2}^{\otimes 2} \rangle. \tag{E23}$$

Finally, a third 6-jet is computed with $\mathbf{x}_2 = \mathbf{0}$. The 6-th coefficient of this jet contains only

$$\langle \partial^6 \mathbf{f}(\mathbf{x}_0), \mathbf{x}_1^{\otimes 6} \rangle. \tag{E24}$$

We obtain

$$90 \langle \partial^4 \mathbf{f}(\mathbf{x}_0), \mathbf{x}_1^{\otimes 2} \otimes \mathbf{x}_2^{\otimes 2} \rangle \quad (\text{E25})$$

by subtracting twice of the 6-th coefficient of the third jet from eq. (E23).

To summarize the procedure, we evaluate the 6-jet three times. The first jet has the input $\mathbf{x}_1 = \mathbf{e}_{d_1}$, $\mathbf{x}_2 = \mathbf{e}_{d_2}$ and $\mathbf{x}_3 = \mathbf{x}_4 = \mathbf{x}_5 = \mathbf{x}_6 = \mathbf{0}$, the second jet has the same input jet apart from $\mathbf{x}_2 = -\mathbf{e}_{d_2}$, and the third 6-jet takes $\mathbf{x}_2 = \mathbf{0}$. Then we add the 6-th coefficient of the first and the second and subtract twice of the 6-th coefficient of the third jet. Dividing by 90 provides the derivative corresponding to the d_1, d_2 term of the biharmonic operator.

Standard Taylor mode would propagate $1 + 18D^2$ vectors through every node, if we already exploit that all jets share \mathbf{x}_0 . our collapsed Taylor mode would pass $1 + 3 + 15D^2$ vectors through every node of the compute graph. This is more costly compared to our approach described before. In addition, until now, the selection of the jet degree and the input coefficients requires substantial human effort.

E.3 Another Example: Mixed Third-order Derivatives

As an additional example, consider computing $\sum_{i=1}^D \sum_{j=1}^D \frac{\partial^3}{\partial x_i^2 \partial x_j} \mathbf{f}(\mathbf{x})$. This example is from [27, §F.2], which describes how to compute these 3rd-order derivatives using 7-jets. The interpolation formula allows using multiple 3-jets instead. We expect it to be favorable as Taylor mode scales polynomially in the derivative order.

Procedure. The goal is to compute $\sum_{i=1}^D \sum_{j=1}^D \frac{\partial^3}{\partial x_i^2 \partial x_j} \mathbf{f}(\mathbf{x})$. We proceed as follows:

1. Formulate the operator in our notation:

$$\sum_{i=1}^D \sum_{j=1}^D \langle \partial^3 \mathbf{f}(\mathbf{x}), \mathbf{e}_i^{\otimes 2} \otimes \mathbf{e}_j \rangle$$

2. Compute the interpolation coefficients $\gamma_{\mathbf{p}, \mathbf{q}}$ for $\mathbf{q} \in \{(3, 0), (2, 1), (1, 2), (0, 3)\}$ and $\mathbf{p} = (2, 1)$: $\gamma_{(2,1)(0,3)} = -8/81$, $\gamma_{(2,1)(1,2)} = 16/27$, $\gamma_{(2,1)(2,1)} = -16/9$, $\gamma_{(2,1)(3,0)} = 32/81$.
3. Apply the interpolation equation (eq. (11)):

$$= \sum_{i=1}^D \sum_{j=1}^D \sum_{\mathbf{q} \in \mathbb{N}^2, \|\mathbf{q}\|_1=3} \langle \partial^3 \mathbf{f}(\mathbf{x}), ([\mathbf{q}]_1 \mathbf{e}_i + [\mathbf{q}]_2 \mathbf{e}_j)^{\otimes 3} \rangle$$

Collapsed Taylor mode can directly applied to these $4D^2$ 3-jets. However, to exploit the full potential some further steps that leverage the structure are required.

4. Expand and manually simplify, using symmetries. The sums for $\gamma_{(2,1)(3,0)}$ and $\gamma_{(2,1)(0,3)}$ are similar; same for $\gamma_{(2,1)(2,1)}$ and $\gamma_{(2,1)(1,2)}$. We only have $2D^2 - 3$ jets:

$$\begin{aligned} &= (\gamma_{(2,1)(3,0)} + \gamma_{(2,1)(0,3)}) \sum_{i=1}^D \sum_{j=1}^D \langle \partial^3 \mathbf{f}(\mathbf{x}), (3\mathbf{e}_i)^{\otimes 3} \rangle \\ &\quad + (\gamma_{(2,1)(2,1)} + \gamma_{(2,1)(1,2)}) \sum_{i=1}^D \sum_{j=1}^D \langle \partial^3 \mathbf{f}(\mathbf{x}), (2\mathbf{e}_i + \mathbf{e}_j)^{\otimes 3} \rangle. \end{aligned}$$

We further observe that the first summation is independent of j :

$$\begin{aligned} &= (\gamma_{(2,1)(3,0)} + \gamma_{(2,1)(0,3)}) D \sum_{i=1}^D \langle \partial^3 \mathbf{f}(\mathbf{x}), (3\mathbf{e}_i)^{\otimes 3} \rangle \\ &\quad + (\gamma_{(2,1)(2,1)} + \gamma_{(2,1)(1,2)}) \sum_{i=1}^D \sum_{j=1}^D \langle \partial^3 \mathbf{f}(\mathbf{x}), (2\mathbf{e}_i + \mathbf{e}_j)^{\otimes 3} \rangle. \end{aligned}$$

Extracting the case $i = j$ from the last term gives our final form

$$\begin{aligned}
&= ((\gamma_{(2,1)(3,0)}D + \gamma_{(2,1)(0,3)}D + \gamma_{(2,1)(2,1)} + \gamma_{(2,1)(1,2)}) \sum_{i=1}^D \langle \partial^3 \mathbf{f}(\mathbf{x}), (3\mathbf{e}_i)^{\otimes 3} \rangle \\
&\quad + (\gamma_{(2,1)(2,1)} + \gamma_{(2,1)(1,2)}) \sum_{i=1}^D \sum_{j=1, j \neq i}^D \langle \partial^3 \mathbf{f}(\mathbf{x}), (2\mathbf{e}_i + \mathbf{e}_j)^{\otimes 3} \rangle.
\end{aligned}$$

This optimized version required D^2 3-jets that can be collapsed.

F PyTorch Benchmark

F.1 Additional Analysis and Impact of `torch.compile`

Here, we compare the theoretically estimated performance improvements based on counting the number of forward-propagated vectors with the empirically measured performance.

The number of propagated vectors is a good empirical performance estimate. To estimate the performance ratio between standard and collapsed Taylor mode, we can use the number of additional vectors both modes propagate forward as we increase either the batch size or the number of Monte-Carlo samples. This is a relatively simplistic proxy; e.g., it assumes that each vector adds the same computational load, which is inaccurate as vectors corresponding to higher coefficients require more work and memory (as the Faà di Bruno formula contains more terms in general). Conversely, while incrementing the MC samples does add additional vectors that are propagated, it does not introduce additional cost to compute or store the derivatives, as they are already computed with just a single sample. Table F2 summarizes the theoretical and empirical ratios. We find them to align quite well, despite the overly simplistic assumptions.

Concrete example. Consider the exact Laplacian. Adding one datum introduces $2 + D$ versus $1 + 2D$ new vectors. For $D = 50$, their ratio is $(2+D)/(1+2D) \approx 0.51$. Empirically, we measure that adding one datum adds **0.56 ms** to standard, and **0.29 ms** to collapsed, Taylor mode (table 1); the ratio of ≈ 0.52 is close.

Compilation reduces memory, but not runtime. In table F3, we repeat the benchmark from table 1 using `torch.compile`. We observe that compiling can further reduce the memory footprint of all approaches for computing the Laplacian and weighted Laplacian, while the runtime remains roughly identical. For the biharmonic operator, we observe that compilation leaves runtime and memory footprint unchanged.

Table F2: **Comparison of theoretical and empirical performance ratios between standard and collapsed Taylor mode.** We list the number of additional vectors that are used when adding another data point (exact) or another Monte-Carlo sample (stochastic). The ratio of vectors offers a good estimate of the empirically measured performance ratio.

| Mode | Add one datum or MC sample | Laplacian ($D = 50$) | Weighted Laplacian ($D = R = 50$) | Biharmonic ($D = 5$) |
|------------|-------------------------------|---------------------------|--|---------------------------|
| Exact | # vectors (standard) | $1 + 2D$ | $1 + 2R$ | $6D^2 - 2D + 1$ |
| | # vectors (collapsed) | $2 + D$ | $2 + R$ | $9/2D^2 - 3/2D + 4$ |
| | Theoretical ratio #/# | 0.51 | 0.51 | 0.77 |
| | Empirical time ratio | 0.52 | 0.51 | 0.76 |
| | Empirical mem. ratio | 0.45 | 0.45 | 0.63 |
| Stochastic | # vectors (standard) | 2 | 2 | 4 |
| | # vectors (collapsed) | 1 | 1 | 3 |
| | Theoretical ratio #/# | 0.5 | 0.5 | 0.75 |
| | Empirical time ratio | 0.51 | 0.51 | 0.74 |
| | Empirical mem. ratio | 0.43 | 0.45 | 0.59 |

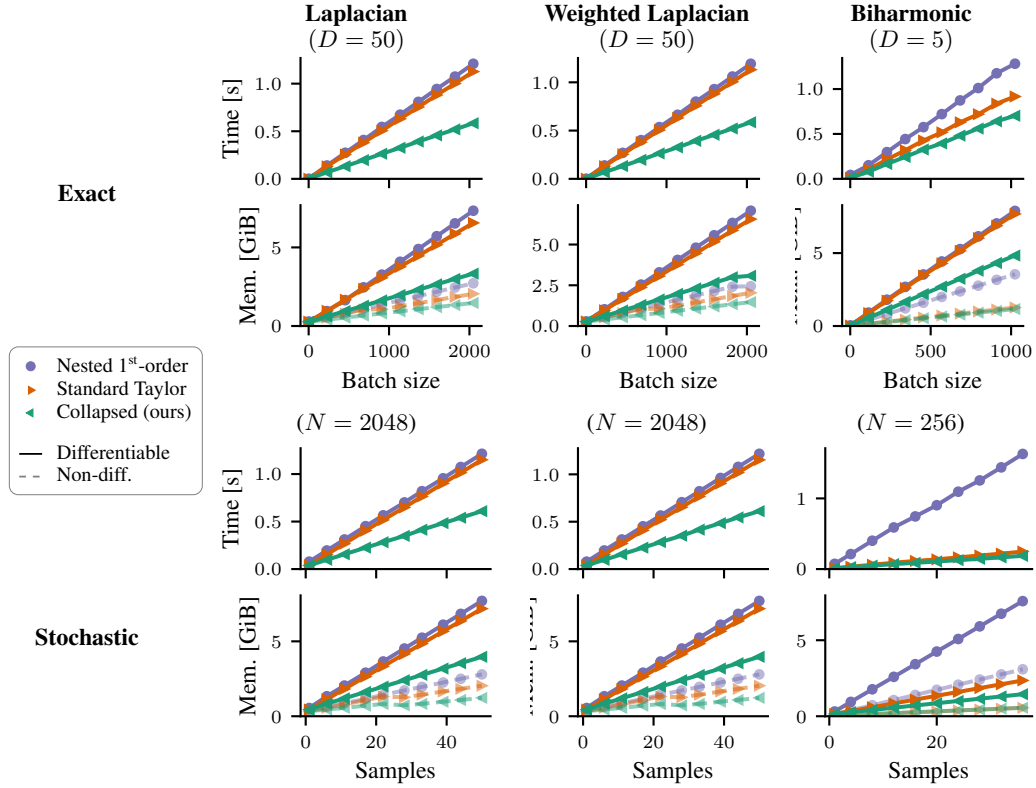


Figure F9: Same as fig. 5, but using torch.compile.

Table F3: Same as table 1, but using torch.compile (i.e. fig. F9 in numbers).

| Mode | Per-datum or -sample cost | Implementation | Laplacian | Weighted Laplacian | Biharmonic via interpolation (E21) |
|------------------------|-------------------------------|-------------------------------|---------------------|---------------------|------------------------------------|
| Exact | Time [ms] | Nested 1 st -order | 0.59 (1.0x) | 0.58 (1.0x) | 1.2 (1.0x) |
| | | Standard Taylor | 0.55 (0.93x) | 0.55 (0.95x) | 0.90 (0.72x) |
| | | Collapsed (ours) | 0.28 (0.48x) | 0.29 (0.49x) | 0.69 (0.55x) |
| | Mem. [MiB] (differentiable) | Nested 1 st -order | 3.6 (1.0x) | 3.4 (1.0x) | 7.9 (1.0x) |
| | | Standard Taylor | 3.1 (0.88x) | 3.1 (0.92x) | 7.7 (0.98x) |
| | | Collapsed (ours) | 1.5 (0.43x) | 1.5 (0.43x) | 4.8 (0.61x) |
| Mem. [MiB] (non-diff.) | Nested 1 st -order | 1.2 (1.0x) | 1.1 (1.0x) | 3.5 (1.0x) | |
| | Standard Taylor | 0.85 (0.69x) | 0.84 (0.73x) | 1.2 (0.36x) | |
| | Collapsed (ours) | 0.60 (0.49x) | 0.60 (0.53x) | 1.1 (0.33x) | |
| Stochastic | Time [ms] | Nested 1 st -order | 23 (1.0x) | 23 (1.0x) | 44 (1.0x) |
| | | Standard Taylor | 23 (0.98x) | 23 (0.98x) | 6.6 (0.15x) |
| | | Collapsed (ours) | 12 (0.50x) | 12 (0.50x) | 4.9 (0.11x) |
| | Mem. [MiB] (differentiable) | Nested 1 st -order | 150 (1.0x) | 150 (1.0x) | 210 (1.0x) |
| | | Standard Taylor | 140 (0.95x) | 140 (0.95x) | 64 (0.30x) |
| | | Collapsed (ours) | 73 (0.49x) | 73 (0.49x) | 38 (0.18x) |
| Mem. [MiB] (non-diff.) | Nested 1 st -order | 50 (1.0x) | 50 (1.0x) | 86 (1.0x) | |
| | Standard Taylor | 33 (0.67x) | 33 (0.67x) | 15 (0.17x) | |
| | Collapsed (ours) | 17 (0.33x) | 17 (0.33x) | 15 (0.17x) | |

Table F4: **Exact weighted Laplacian for different ranks of the weightings.** The lower the rank, the lower the memory and time consumption. Both scale approximately linear with the rank—with stronger deviations for small ranks—as predicted by our theoretical analysis based on the number of forward-propagated coefficients. The ‘Full-rank’ column is identical to the ‘Weighted Laplacian’ columns in Tables 1 and F3.

| compile | Per-datum or -sample cost | Implementation | Weighted Laplacian ($D = 50$) | | |
|---------|-----------------------------|-------------------------------|---------------------------------|--------------------------|----------------------|
| | | | Full-rank (D) | Half-full rank ($D/2$) | Low-rank ($D/10$) |
| ✓ | Time [ms] | Nested 1 st -order | 0.58 (1.0x) | 0.30 (1.0x) | 0.082 (1.0x) |
| | | Standard Taylor | 0.55 (0.95x) | 0.28 (0.92x) | 0.062 (0.76x) |
| | | Collapsed (ours) | 0.29 (0.49x) | 0.15 (0.49x) | 0.040 (0.49x) |
| | Mem. [MiB] (differentiable) | Nested 1 st -order | 3.4 (1.0x) | 1.8 (1.0x) | 0.43 (1.0x) |
| | | Standard Taylor | 3.1 (0.92x) | 1.6 (0.90x) | 0.33 (0.78x) |
| | | Collapsed (ours) | 1.5 (0.43x) | 0.80 (0.46x) | 0.21 (0.50x) |
| | Mem. [MiB] (non-diff.) | Nested 1 st -order | 1.1 (1.0x) | 0.62 (1.0x) | 0.15 (1.0x) |
| | | Standard Taylor | 0.84 (0.73x) | 0.47 (0.76x) | 0.12 (0.82x) |
| | | Collapsed (ours) | 0.60 (0.53x) | 0.31 (0.49x) | 0.073 (0.48x) |
| ✗ | Time [ms] | Nested 1 st -order | 0.60 (1.0x) | 0.31 (1.0x) | 0.084 (1.0x) |
| | | Standard Taylor | 0.57 (0.94x) | 0.29 (0.92x) | 0.065 (0.78x) |
| | | Collapsed (ours) | 0.29 (0.48x) | 0.15 (0.49x) | 0.042 (0.51x) |
| | Mem. [MiB] (differentiable) | Nested 1 st -order | 4.4 (1.0x) | 2.2 (1.0x) | 0.53 (1.0x) |
| | | Standard Taylor | 4.6 (1.0x) | 2.4 (1.0x) | 0.60 (1.1x) |
| | | Collapsed (ours) | 2.1 (0.47x) | 1.1 (0.50x) | 0.39 (0.74x) |
| | Mem. [MiB] (non-diff.) | Nested 1 st -order | 2.2 (1.0x) | 1.1 (1.0x) | 0.26 (1.0x) |
| | | Standard Taylor | 1.2 (0.54x) | 0.60 (0.54x) | 0.14 (0.53x) |
| | | Collapsed (ours) | 0.90 (0.41x) | 0.46 (0.41x) | 0.11 (0.41x) |

F.2 Rank-deficient Weighted Laplacian

In the main text we use a weighted Laplacian with a full-rank weight matrix (i.e., $R := \text{rank}(D) = D$). Since the weight matrix has full rank, the weighted Laplacian is as expensive as the unweighted Laplacian, and this is confirmed by our experiments. To show that the weight matrix’s rank indeed affects the cost, we experiment with a rank-deficient weight matrix in this section and also consider the ranks $R \in \{D/2, D/10\}$. Table F4 contains the results of this analysis. We observe that going from full to half-full rank roughly halves both the runtime and memory consumption for all implementations. For small ranks, this linear relationship weakens because the fraction of computations that do not scale with R grows.

G JAX Benchmark

This section presents experiments which show that the graph simplifications we propose to collapse standard Taylor mode are currently not applied by the `jit` compiler in JAX.

Comparing JAX implementations. Similar to our PyTorch experiment in §4, we compare three implementations of the Laplacian in JAX (all compiled with `jax.jit`):

1. **Nested 1st-order AD** computes the Hessian using `jax.hessian`, which relies on forward-over-reverse mode, then traces it.
2. **Standard Taylor mode** propagates multiple univariate Taylor polynomials, each of which computes one element of the Hessian diagonal, then sums them to obtain the Laplacian. This is implemented with `jax.experimental.jet.jet` and `jax.vmap`.
3. **Collapsed Taylor mode** relies on the forward Laplacian implementation in JAX provided by the `folx` library [12] and implements our proposed collapsed Taylor mode for the specific case of the Laplacian. `folx` also enables leveraging sparsity in the tensors, which is

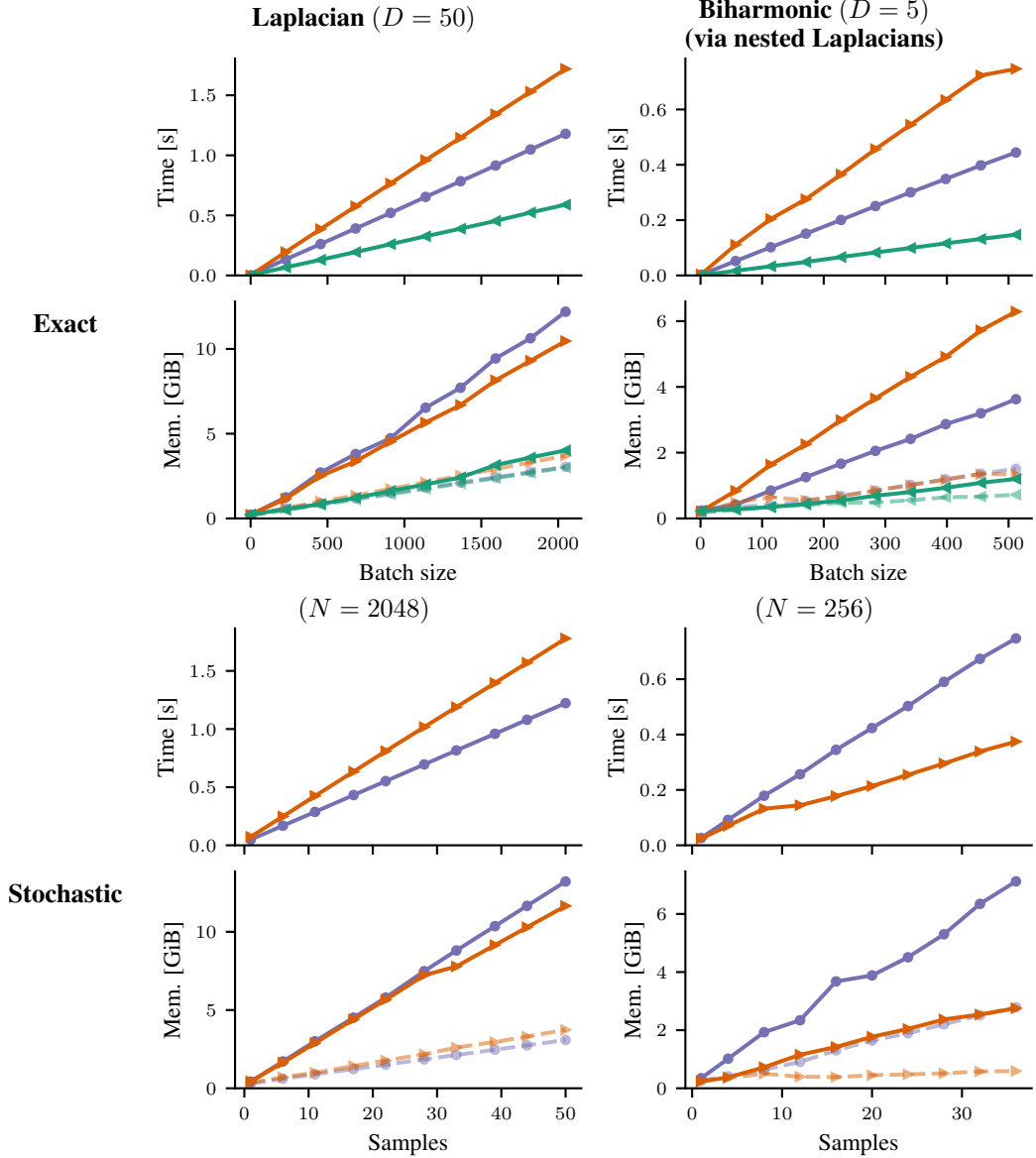


Figure G10: **JAX’s jit compiler does not apply our graph simplifications to standard Taylor mode.** Colors: Collapsed Taylor mode, standard Taylor mode, and nested first-order automatic differentiation, opaque memory consumptions are for non-differentiable computations. Results are on GPU and we use a $D \rightarrow 768 \rightarrow 768 \rightarrow 512 \rightarrow 512 \rightarrow 1$ MLP with tanh activations, varying the batch size. For each approach, we fit a line to the data and report the slope in table G5 to quantify the relative speedup and memory reduction.

beneficial for architectures in VMC. To disentangle runtime improvements from sparsity detection versus collapsing Taylor coefficient, we disable `folx`’s sparsity detection.

For the biharmonic operator, we simply nest the Laplacian implementations.

We only investigate computing the exact Laplacian, as the forward Laplacian in `folx` currently does not support stochastic computation. We use the same neural network architecture as for our PyTorch experiments, fix the input dimension to $D = 50$ and vary the batch size, recording the runtime and peak memory with the same protocol as described in the main text. JAX is purely functional and therefore does not have a mechanism to build up a differentiable computational graph similar to evaluating a function in PyTorch where some leaves have `requires_grad=True`. To approximate the

Table G5: **JAX Benchmark from fig. G10 in numbers.** We fit linear functions and report their slopes, i.e., how much runtime and memory increase when incrementing the batch size. All numbers are shown with two significant digits and bold values are best according to parenthesized values.

| Mode | Per-datum or sample cost | Implementation | Laplacian | Biharmonic (via nested Laplacians) |
|------------------------|-------------------------------|-------------------------------|---------------------|------------------------------------|
| Exact | Time [ms] | Nested 1 st -order | 0.58 (1.0x) | 0.87 (1.0x) |
| | | Standard Taylor | 0.84 (1.5x) | 1.5 (1.7x) |
| | | Collapsed (ours) | 0.29 (0.50x) | 0.29 (0.33x) |
| | Mem. [MiB] (differentiable) | Nested 1 st -order | 6.0 (1.0x) | 7.0 (1.0x) |
| | | Standard Taylor | 5.1 (0.85x) | 12 (1.8x) |
| | | Collapsed (ours) | 1.9 (0.32x) | 2.0 (0.29x) |
| Mem. [MiB] (non-diff.) | Nested 1 st -order | 1.4 (1.0x) | 2.7 (1.0x) | |
| | Standard Taylor | 1.7 (1.2x) | 2.2 (0.83x) | |
| | Collapsed (ours) | 1.4 (1.0x) | 1.1 (0.39x) | |
| Stochastic | Time [ms] | Nested 1 st -order | 24 (1.0x) | 21 (1.0x) |
| | | Standard Taylor | 35 (1.5x) | 9.5 (0.46x) |
| | | Collapsed (ours) | Not implemented | Not implemented |
| | Mem. [MiB] (differentiable) | Nested 1 st -order | 270 (1.0x) | 190 (1.0x) |
| | | Standard Taylor | 230 (0.87x) | 77 (0.40x) |
| | | Collapsed (ours) | Not implemented | Not implemented |
| Mem. [MiB] (non-diff.) | Nested 1 st -order | 58 (1.0x) | 77 (1.0x) | |
| | Standard Taylor | 71 (1.2x) | 7.9 (0.10x) | |
| | Collapsed (ours) | Not implemented | Not implemented | |

peak memory of computing a differentiable Laplacian in JAX, we measure the peak memory of first computing the Laplacian, then evaluating the gradient w.r.t. the neural network’s parameters which backpropagates through the same computation graph built by PyTorch.

Results (Laplacian). The left column of fig. G10 visualizes the performance of the three implementations. We fit linear functions to each of them and report the cost incurred by adding one more datum to the batch in table G5. From them, we draw the following conclusions:

1. **Performance is consistent between PyTorch and JAX.** Although our PyTorch implementation does not leverage compilation, the values reported in tables 1 and G5 are consistent and only in rare cases differ by a factor of more than two. This confirms that our PyTorch-based implementation of Taylor mode is reasonably efficient, and that the presented performance results in the main text are transferable to other frameworks like JAX.
2. **Our implementation of collapsed Taylor mode based on graph rewrites in PyTorch achieves consistent speed-up with the Laplacian-specific implementation in JAX.** Specifically, we observe that collapsed Taylor mode/forward Laplacian use roughly half the runtime of nested 1st-order AD (compare tables 1 and G5). This supports our argument that our collapsed Taylor is indeed a generalization of the forward Laplacian, i.e., the latter does not employ additional tricks (leveraging sparsity could also be applied to our approach but we are not aware of a drop-in implementation). It also illustrates that the savings we report in PyTorch carry over to other frameworks like JAX.
3. **JAX’s jit compiler is unable to apply the graph rewrites we propose in this work.** If the JAX compiler was able to perform our proposed graph rewrites, then the jit-compiled standard Taylor mode should yield similar performance than the forward Laplacian. However, we observe a clear performance gap in runtime and memory, from which we conclude that the compilation did not collapse the Taylor coefficients. Our contribution is to point out that such rewrites could easily be added to the compiler’s ability to unlock these performance gains at zero user overhead.

Results (biharmonic operator). For the biharmonic operator (right column of fig. G10 and table G5), we conclude that (i) the most efficient way to compute biharmonics is by nesting Laplacians (compare with table 1 where Taylor mode uses the approach for general linear differential operators) and (ii) that nesting Taylor mode Laplacians is more efficient than nesting 1st-order AD Laplacians, while also allowing to apply our collapsing technique.

H Numerical Complexity and Error Analysis

Setup. To illustrate the numerical properties of our proposed collapsed Taylor mode, we consider a two-layered MLP with element-wise tanh activation $\phi : \mathbb{R}^I \rightarrow \mathbb{R}^I$. The MLP is denoted by $\mathbf{f} := \mathbf{g} \circ \phi \circ \mathbf{h}$. The two linear layers are given as $\mathbf{h} : \mathbb{R}^D \rightarrow \mathbb{R}^I$, $\mathbf{h}(\mathbf{x}_0) = \mathbf{W}_1 \mathbf{x}_0 + \mathbf{b}_1$ and $\mathbf{g} : \mathbb{R}^I \rightarrow \mathbb{R}^C$, $\mathbf{g}(\phi_0) = \mathbf{W}_2 \phi_0 + \mathbf{b}_2$, with weights $\mathbf{W}_1 \in \mathbb{R}^{I \times D}$, $\mathbf{W}_2 \in \mathbb{R}^{C \times I}$ and bias $\mathbf{b}_1 \in \mathbb{R}^I$, $\mathbf{b}_2 \in \mathbb{R}^C$. Below we compare the computational and storage complexity, as well as stability for evaluating the sum of the second coefficients $\sum_{r=1}^R \langle \partial^2 \mathbf{f}(\mathbf{x}_0), \mathbf{v}_i^{\otimes 2} \rangle = \sum_{r=1}^R \mathbf{g}_{2,r}$ (see eq. (5)) between collapsed and standard Taylor mode. For this toy example we show (i) collapsing uses less operations and (ii) both methods are similarly stable based on our simplified error analysis.

Computational & storage complexity. Both vanilla and collapsed Taylor mode evaluate the function values $(\mathbf{h}_0, \phi_0, \mathbf{g}_0)$ and the first derivatives $(\{\mathbf{h}_{1,r}, \phi_{1,r}, \mathbf{g}_{1,r}\})$ by propagating $1 + R$ coefficients at each layer

$$\left(\begin{array}{l} \mathbf{h}_0 = \mathbf{W}_1 \mathbf{x}_0 + \mathbf{b}_1 \\ \{\mathbf{h}_{1,r}\} = \{\langle \mathbf{W}_1, \mathbf{x}_{1,r} \rangle\} \end{array} \right) \xrightarrow{(3)} \left(\begin{array}{l} \phi_0 = \phi(\mathbf{h}_0) \\ \{\phi_{1,r}\} = \{\langle \partial \phi(\mathbf{h}_0), \mathbf{h}_{1,r} \rangle\} \end{array} \right) \xrightarrow{(3)} \left(\begin{array}{l} \mathbf{g}_0 = \mathbf{W}_2 \phi_0 + \mathbf{b}_2 \\ \{\mathbf{g}_{1,r}\} = \{\langle \mathbf{W}_2, \phi_{1,r} \rangle\} \end{array} \right)$$

with $\partial \phi(\mathbf{h}_0) = \partial \tanh(\mathbf{h}_0) = \text{diag}(\mathbf{1} - \phi_0^{\odot 2}) \in \mathbb{R}^{I \times I}$ the tanh-activation layer’s Jacobian. The propagation costs $1 + R$ matrix-vector multiplications with \mathbf{W}_1 , $1 + R$ matrix-vector multiplications with \mathbf{W}_2 , R Hadamard products with the derivative of ϕ (since $\langle \text{diag}(\mathbf{a}), \mathbf{h}_{1,r} \rangle = \mathbf{a} \odot \mathbf{h}_{1,r}$), and one Hadamard product to compute $\partial \phi(\mathbf{h}_0)$. Additionally, there is one vector addition with the bias \mathbf{b}_1 , one vector addition with \mathbf{b}_2 , one vector subtraction in $\partial \phi(\mathbf{h}_0)$ (counted as vector addition), as well as the evaluation of $\phi(\mathbf{h}_0)$. $3 + 3R$ vectors are stored.

For the second derivatives, vanilla Taylor mode propagates R vectors

$$\left(\{\mathbf{h}_{2,r}\} = \{\langle \mathbf{W}_1, \mathbf{x}_{2,r} \rangle\} \right) \xrightarrow{(3)} \left(\{\phi_{2,r}\} = \{\langle \partial^2 \phi(\mathbf{h}_0), \mathbf{h}_{1,r}^{\otimes 2} \rangle + \langle \partial \phi(\mathbf{h}_0), \mathbf{h}_{2,r} \rangle\} \right) \\ \xrightarrow{(3)} \left(\{\mathbf{g}_{2,r}\} = \{\langle \mathbf{W}_2, \phi_{2,r} \rangle\} \right)$$

with activation Hessian $\partial^2 \phi(\mathbf{h}_0) \in \mathbb{R}^{I \times I \times I}$ of entries $[\partial^2 \phi(\mathbf{h}_0)]_{i,j,k} = [-2\phi_0 \odot (\mathbf{1} - \phi_0^{\odot 2})]_i \delta_{i,j,k}$ and contraction $\langle \partial^2 \phi(\mathbf{h}_0), \mathbf{h}_{1,r}^{\otimes 2} \rangle = -2\phi_0 \odot (\mathbf{1} - \phi_0^{\odot 2}) \odot \mathbf{h}_{1,r}^{\odot 2}$. These vectors are summed up to get the result $\sum_{r=1}^R \langle \partial^2 \mathbf{f}(\mathbf{x}_0), \mathbf{v}_i^{\otimes 2} \rangle = \sum_{r=1}^R \mathbf{g}_{2,r}$. This costs $2R$ matrix-vector products with the weights, $1 + 3R$ Hadamard products, $2R - 1$ vector additions, and a single scalar multiplication.

Table H6: **Comparison of theoretical computational and storage complexity** between standard Taylor mode and collapsed Taylor mode for a two-layer MLP computing the sum $\sum_{r=1}^R \langle \partial^2 \mathbf{f}(\mathbf{x}_0), \mathbf{v}_r^{\otimes 2} \rangle$.

| Computational Complexity | | |
|--------------------------|-----------------|------------------|
| Operation | Standard Taylor | Collapsed (ours) |
| # Matrix-vector products | $4R + 2$ | $2R + 4$ |
| # Hadamard products | $4R + 2$ | $3R + 3$ |
| # Vector additions | $2R + 2$ | $2R + 2$ |
| # Scalar multiplications | 1 | 1 |
| # Activation evaluations | I | I |
| Storage Complexity | | |
| # Vectors stored | $6R + 3$ | $3R + 6$ |

In contrast, collapsed Taylor mode propagates only a single summed vector

$$\begin{aligned} \left(\sum_{r=1}^R \mathbf{h}_{2,r} = \left\langle \mathbf{W}_1, \sum_{r=1}^R \mathbf{x}_{2,r} \right\rangle \right) &\stackrel{(3)}{\rightarrow} \left(\sum_{r=1}^R \phi_{2,r} = \sum_{r=1}^R \langle \partial^2 \phi(\mathbf{h}_0), \mathbf{h}_{1,r}^{\otimes 2} \rangle + \left\langle \partial \phi(\mathbf{h}_0), \sum_{r=1}^R \mathbf{h}_{2,r} \right\rangle \right) \\ &\stackrel{(3)}{\rightarrow} \left(\sum_{r=1}^R \mathbf{g}_{2,r} = \left\langle \mathbf{W}_2, \sum_{r=1}^R \phi_{2,r} \right\rangle \right). \end{aligned}$$

This costs two matrix-vector products, $2 + 2R$ Hadamard products, $2R - 1$ vector additions, and a single scalar multiplication. Table H6 summarizes the accumulated costs.

Error analysis. For our numerical experiments, the result of all implementations (nested 1st-order and standard/collapsed Taylor mode) was always checked to be close. To supplement this experimental error analysis, we sketch a simplified error analysis below. We assume that there are error-prone first- and second-order inputs $\{\mathbf{x}_{1,r} + \varepsilon_{1,r}\}_r$ and $\{\mathbf{x}_{2,r} + \varepsilon_{2,r}\}_r$ with errors $\{\varepsilon_{1,r}, \varepsilon_{2,r}\}_{r=1}^R$ that can be seen as the error of previous propagation steps. An error-prone \mathbf{x}_0 would complicate our brief discussion too much and is ignored here. We consider again $\mathbf{f} = \mathbf{g} \circ \phi \circ \mathbf{h}$. The error-influenced coefficients are denoted $\mathbf{g}_{2,r}^\varepsilon$.

Using vanilla Taylor mode, the erroneous result is

$$\begin{aligned} \sum_{r=1}^R \mathbf{g}_{2,r}^\varepsilon &= \sum_{r=1}^R \left(\left\langle \mathbf{W}_2, \left\langle \partial^2 \phi(\mathbf{h}_0), \langle \mathbf{W}_1, \mathbf{x}_{1,r} + \varepsilon_{1,r} \rangle^{\otimes 2} \right\rangle + \left\langle \partial \phi(\mathbf{h}_0), \langle \mathbf{W}_1, \mathbf{x}_{2,r} + \varepsilon_{2,r} \rangle \right\rangle \right) \\ &= \sum_{r=1}^R \mathbf{g}_{2,r} \\ &\quad + \sum_{r=1}^R \left(\left\langle \mathbf{W}_2, \left\langle \partial^2 \phi(\mathbf{h}_0), \langle \mathbf{W}_1, \mathbf{x}_{1,r} \rangle \otimes \langle \mathbf{W}_1, \varepsilon_{1,r} \rangle \right\rangle \right) \\ &\quad + \left\langle \mathbf{W}_2, \left\langle \partial^2 \phi(\mathbf{h}_0), \langle \mathbf{W}_1, \varepsilon_{1,r} \rangle \otimes \langle \mathbf{W}_1, \mathbf{x}_{1,r} \rangle \right\rangle \right) \\ &\quad + \left\langle \mathbf{W}_2, \left\langle \partial^2 \phi(\mathbf{h}_0), \langle \mathbf{W}_1, \varepsilon_{1,r} \rangle^{\otimes 2} \right\rangle \right\rangle + \left\langle \mathbf{W}_2, \left\langle \partial \phi(\mathbf{h}_0), \langle \mathbf{W}_1, \varepsilon_{2,r} \rangle \right\rangle \right) \\ &= \sum_{r=1}^R \mathbf{g}_{2,r} + \Delta \mathbf{g}_{2,R}^S + \sum_{r=1}^R \left\langle \mathbf{W}_2, \left\langle \partial \phi(\mathbf{h}_0), \langle \mathbf{W}_1, \varepsilon_{2,r} \rangle \right\rangle \right). \end{aligned}$$

All errors related to the first-order coefficients are summarized in

$$\begin{aligned} \Delta \mathbf{g}_{2,R}^S &:= \sum_{r=1}^R \left(\left\langle \mathbf{W}_2, \left\langle \partial^2 \phi(\mathbf{h}_0), \langle \mathbf{W}_1, \mathbf{x}_{1,r} \rangle \otimes \langle \mathbf{W}_1, \varepsilon_{1,r} \rangle \right\rangle \right) \right. \\ &\quad + \left\langle \mathbf{W}_2, \left\langle \partial^2 \phi(\mathbf{h}_0), \langle \mathbf{W}_1, \varepsilon_{1,r} \rangle \otimes \langle \mathbf{W}_1, \mathbf{x}_{1,r} \rangle \right\rangle \right) \\ &\quad \left. + \left\langle \mathbf{W}_2, \left\langle \partial^2 \phi(\mathbf{h}_0), \langle \mathbf{W}_1, \varepsilon_{1,r} \rangle^{\otimes 2} \right\rangle \right\rangle \right). \end{aligned}$$

The collapsed Taylor mode results in

$$\begin{aligned} \sum_{r=1}^R \mathbf{g}_{2,r}^\varepsilon &= \left\langle \mathbf{W}_2, \sum_{r=1}^R \left(\left\langle \partial^2 \phi(\mathbf{h}_0), \langle \mathbf{W}_1, \mathbf{x}_{1,r} + \varepsilon_{1,r} \rangle^{\otimes 2} \right\rangle \right) \right\rangle \\ &\quad + \left\langle \mathbf{W}_2, \left\langle \partial \phi(\mathbf{h}_0), \left\langle \mathbf{W}_1, \sum_{r=1}^R (\mathbf{x}_{2,r} + \varepsilon_{2,r}) \right\rangle \right\rangle \right\rangle \end{aligned}$$

$$\begin{aligned}
&= \sum_{r=1}^R \mathbf{g}_{2,r} \\
&\quad + \left\langle \mathbf{W}_2, \sum_{r=1}^R \left(\langle \partial^2 \phi(\mathbf{h}_0), \langle \mathbf{W}_1, \mathbf{x}_{1,r} \rangle \otimes \langle \mathbf{W}_1, \boldsymbol{\varepsilon}_{1,r} \rangle \rangle + \langle \partial^2 \phi(\mathbf{h}_0), \langle \mathbf{W}_1, \boldsymbol{\varepsilon}_{1,r} \rangle \otimes \langle \mathbf{W}_1, \mathbf{x}_{1,r} \rangle \rangle \right. \right. \\
&\quad \quad \left. \left. + \langle \partial^2 \phi(\mathbf{h}_0), \langle \mathbf{W}_1, \boldsymbol{\varepsilon}_{1,r} \rangle^{\otimes 2} \rangle \right) \right\rangle \\
&\quad + \left\langle \mathbf{W}_2, \left\langle \partial \phi(\mathbf{h}_0), \left\langle \mathbf{W}_1, \sum_{r=1}^R \boldsymbol{\varepsilon}_{2,r} \right\rangle \right\rangle \right\rangle \\
&= \sum_{r=1}^R \mathbf{g}_{2,r} + \Delta \mathbf{g}_{2,R}^C + \left\langle \mathbf{W}_2, \left\langle \partial \phi(\mathbf{h}_0), \left\langle \mathbf{W}_1, \sum_{r=1}^R \boldsymbol{\varepsilon}_{2,r} \right\rangle \right\rangle \right\rangle,
\end{aligned}$$

where the first-order errors are collected in

$$\begin{aligned}
\Delta \mathbf{g}_{2,R}^C := &\left\langle \mathbf{W}_2, \sum_{r=1}^R \left(\langle \partial^2 \phi(\mathbf{h}_0), \langle \mathbf{W}_1, \mathbf{x}_{1,r} \rangle \otimes \langle \mathbf{W}_1, \boldsymbol{\varepsilon}_{1,r} \rangle \right. \right. \\
&\quad \left. \left. + \langle \partial^2 \phi(\mathbf{h}_0), \langle \mathbf{W}_1, \boldsymbol{\varepsilon}_{1,r} \rangle \otimes \langle \mathbf{W}_1, \mathbf{x}_{1,r} \rangle \rangle + \langle \partial^2 \phi(\mathbf{h}_0), \langle \mathbf{W}_1, \boldsymbol{\varepsilon}_{1,r} \rangle^{\otimes 2} \rangle \right) \right\rangle.
\end{aligned}$$

Error analysis (summary and discussion). Without considering floating-point operations, the errors are equivalent. This is not surprising, since our collapsing method is mathematically equivalent to the standard Taylor mode on the same input coefficients.

Incorporating floating-point operations for the function evaluations, inner product, tensor product, and summations would greatly complicate the discussion, which is not part of the paper. Still, the error could be split into the same three parts for both vanilla and collapsed Taylor mode. For the first-order errors $\Delta \mathbf{g}_{2,R}^S$ and $\Delta \mathbf{g}_{2,R}^C$, however, even with floating-point operations, the errors are structurally similar, since apart from the most outer inner product (with \mathbf{W}_2) and the summation, all operations are done in the same order. In practice, we would expect smaller errors for the collapsing method due to the reduced number of operations. The second error term, which collects the error of the second-order coefficients, could also reduce the accumulation of error terms. Of course, the actual condition and input, and output dimensions of the matrices are crucial. Theoretically, this could even lead to a similar error asymptotically. If inputs are small, one could argue that catastrophic cancellations are more likely to happen in our case, since we sum first. But note that those cancellations are then also likely to happen in the standard Taylor mode, because weight matrices are often normalized, and the outputs of the activation functions are small if the input is small.

We plan to investigate this more rigorously in the future.

I Connections of Collapsed Taylor Mode to Existing Methods

Here, we make the connection of collapsed Taylor mode to the forward Laplacian [21] and the randomized estimation of the Laplacian via Hutchinson’s trace estimator [18] from [27] explicit.

I.1 Connection to Randomized Laplacian via Hutchinson’s Trace Estimator

For simplicity, we consider a vector-to-scalar function $f : \mathbb{R}^D \rightarrow \mathbb{R}, \mathbf{x} \mapsto f(\mathbf{x})$ (the general vector-to-vector case is straightforward but requires more notation) whose Laplacian is

$$\Delta f(\mathbf{x}) = \text{Tr}(\nabla^2 f(\mathbf{x})) = \sum_{d=1}^D [\nabla^2 f(\mathbf{x})]_{d,d} = \sum_{d=1}^D \mathbf{e}_d^\top \nabla^2 f(\mathbf{x}) \mathbf{e}_d,$$

with $\nabla^2 f(\mathbf{x}) \in \mathbb{R}^{D \times D}$ the Hessian of f evaluated at \mathbf{x} . Because the Laplacian can be expressed as trace of the Hessian, we can use Hutchinson’s trace estimator [18] to estimate it via Hessian-vector products with random vectors. Specifically, for any matrix $\mathbf{A} \in \mathbb{R}^{D \times D}$ and a distribution $p(\mathbf{v})$ over a

vector \mathbf{v} with unit covariance ($\mathbb{E}[\mathbf{v}\mathbf{v}^\top] = \mathbf{I}_D$) we can use the cyclic property of the trace and linearity of the expectation to write

$$\text{Tr}(\mathbf{A}) = \text{Tr}(\mathbf{A}\mathbf{I}_D) = \text{Tr}(\mathbf{A}\mathbb{E}[\mathbf{v}\mathbf{v}^\top]) = \mathbb{E}[\text{Tr}(\mathbf{A}\mathbf{v}\mathbf{v}^\top)] = \mathbb{E}[\text{Tr}(\mathbf{v}^\top \mathbf{A} \mathbf{v})].$$

Then, we can compute an unbiased estimate of the right hand side by drawing S vectors $\mathbf{v}_1, \mathbf{v}_2, \dots, \mathbf{v}_S \sim p(\mathbf{v})$ and evaluating the Monte-Carlo estimator

$$\text{Tr}(\mathbf{A}) \approx \frac{1}{S} \sum_{s=1}^S \mathbf{v}_s^\top \mathbf{A} \mathbf{v}_s.$$

Applied to the Hessian, we can estimate the Laplacian of f as

$$\Delta f(\mathbf{x}) \approx \frac{1}{S} \sum_{s=1}^S \mathbf{v}_s^\top \nabla^2 f(\mathbf{x}) \mathbf{v}_s.$$

Using our tensor notation, we can rewrite this into a sum of terms involving $\langle \partial^2 f(\mathbf{x}), \mathbf{v}_s^{\otimes 2} \rangle$, which can be computed with **vanilla Taylor mode** using S 2-jets (see eq. (4)):

$$= \frac{1}{S} \sum_{s=1}^S \sum_{i,j=1}^D [\partial^2 f(\mathbf{x})]_{i,j} [\mathbf{v}_s]_i [\mathbf{v}_s]_j = \frac{1}{S} \sum_{s=1}^S \langle \partial^2 f(\mathbf{x}), \mathbf{v}_s^{\otimes 2} \rangle.$$

Instead of propagating then summing the 2-jets, we can also sum the vectors and then propagate the sum (assuming we have a composition, see eq. (D16)), which is our proposed **collapsed Taylor mode**:

$$= \frac{1}{S} \left\langle \partial^2 f(\mathbf{x}), \sum_{s=1}^S \mathbf{v}_s^{\otimes 2} \right\rangle.$$

I.2 Connection to the Forward Laplacian

We start by writing out the propagation rules of the forward Laplacian (eqs. (5-7) in Li et al. [21]) for a function $f = g \circ \mathbf{h}$ with $g : \mathbb{R}^C \rightarrow \mathbb{R}$ whose input we denote by $\mathbf{h}_0 \in \mathbb{R}^C$. The forward propagation consumes $\mathbf{h}_0 = \mathbf{h}(\mathbf{x}_0)$, the Jacobian $\nabla_{\mathbf{x}_0} \mathbf{h}_0 = \nabla_{\mathbf{x}_0} \mathbf{h}(\mathbf{x}_0) \in \mathbb{R}^{D \times C}$, and the Laplacian $\Delta_{\mathbf{x}_0} \mathbf{h}_0 = \Delta_{\mathbf{x}_0} \mathbf{h}(\mathbf{x}_0) \in \mathbb{R}^C$:

$$\begin{pmatrix} \mathbf{h}_0 & \in \mathbb{R}^C \\ \nabla_{\mathbf{x}_0} \mathbf{h}_0 & \in \mathbb{R}^{D \times C} \\ \Delta_{\mathbf{x}_0} \mathbf{h}_0 & \in \mathbb{R}^C \end{pmatrix} \rightarrow \begin{pmatrix} g_0 = g(\mathbf{h}_0) & \in \mathbb{R} \\ \nabla_{\mathbf{x}_0} g_0 = (\nabla_{\mathbf{x}_0} \mathbf{h}_0) (\nabla_{\mathbf{h}_0} g_0) & \in \mathbb{R}^D \\ \Delta_{\mathbf{x}_0} g_0 = (\nabla_{\mathbf{h}_0} g_0)^\top \Delta \mathbf{h}_0 + \text{Tr}((\nabla_{\mathbf{x}_0} \mathbf{h}_0)^\top (\nabla_{\mathbf{x}_0} \mathbf{h}_0) \nabla_{\mathbf{h}_0} g_0) & \in \mathbb{R} \end{pmatrix}.$$

Let us rewrite this in terms of rows of the Jacobian $[\nabla_{\mathbf{x}_0} \mathbf{h}_0]_{d,:} \in \mathbb{R}^C$ (where the colon subscript denotes a slice):

$$\begin{pmatrix} \mathbf{h}_0 \\ \{[\nabla_{\mathbf{x}_0} \mathbf{h}_0]_{d,:}\}_{d=1}^D \\ \Delta_{\mathbf{x}_0} \mathbf{h}_0 \end{pmatrix} \rightarrow \begin{pmatrix} g_0 = g(\mathbf{h}_0) \\ \{[\nabla_{\mathbf{x}_0} g_0]_{d,:} = [\nabla_{\mathbf{x}_0} \mathbf{h}_0]_{d,:} (\nabla_{\mathbf{h}_0} g_0)\}_{d=1}^D \\ \Delta_{\mathbf{x}_0} g_0 = (\nabla_{\mathbf{h}_0} g_0)^\top \Delta \mathbf{h}_0 + \sum_{d=1}^D [\nabla_{\mathbf{x}_0} \mathbf{h}_0]_{d,:} \nabla_{\mathbf{h}_0}^2 g_0 [\nabla_{\mathbf{x}_0} \mathbf{h}_0]_{d,:}^\top \end{pmatrix}.$$

In our tensor notation, this translates to

$$\begin{pmatrix} \mathbf{h}_0 \\ \{[\nabla_{\mathbf{x}_0} \mathbf{h}_0]_{d,:}\}_{d=1}^D \\ \Delta_{\mathbf{x}_0} \mathbf{h}_0 \end{pmatrix} \rightarrow \begin{pmatrix} g_0 = g(\mathbf{h}_0) \\ \{[\nabla_{\mathbf{x}_0} g_0]_{d,:} = \langle \partial g(\mathbf{h}_0), [\nabla_{\mathbf{x}_0} \mathbf{h}_0]_{d,:} \rangle\}_{d=1}^D \\ \Delta_{\mathbf{x}_0} g_0 = \langle \partial g(\mathbf{h}_0), \Delta \mathbf{h}_0 \rangle + \sum_{d=1}^D \langle \partial g(\mathbf{h}_0), [\nabla_{\mathbf{x}_0} \mathbf{h}_0]_{d,:}^{\otimes 2} \rangle \end{pmatrix}.$$

To obtain the connection to Taylor mode, we define $[\nabla_{\mathbf{x}_0} \mathbf{h}_0]_{d,:} = \mathbf{h}_{1,d}$ and $\Delta_{\mathbf{x}_0} \mathbf{h}_0 = \sum_d \mathbf{h}_{2,d}$ and $[\nabla_{\mathbf{x}_0} g_0]_{d,:} = g_{1,d}$ and $\Delta_{\mathbf{x}_0} g_0 = \sum_d g_{2,d}$, which allows us to rewrite the forward Laplacian as

$$\begin{pmatrix} \mathbf{h}_0 \\ \{\mathbf{h}_{1,d}\}_{d=1}^D \\ \sum_d \mathbf{h}_{2,d} \end{pmatrix} \rightarrow \begin{pmatrix} g_0 = g(\mathbf{h}_0) \\ \{g_{1,d} = \langle \partial g(\mathbf{h}_0), \mathbf{h}_{1,d} \rangle\}_{d=1}^D \\ \sum_d g_{2,d} = \langle \partial g(\mathbf{h}_0), \sum_d \mathbf{h}_{2,d} \rangle + \sum_{d=1}^D \langle \partial g(\mathbf{h}_0), \mathbf{h}_{1,d}^{\otimes 2} \rangle \end{pmatrix}.$$

This yields our collapsed Taylor mode propagation: the first equation is simply the forward pass, the second equation propagates the first-order derivatives along D directions, and the last equation propagates the collapsed second-order derivatives, as described by setting $K = 2$ in Equation (6).